12-2008

Particle Characterization and Concentration Using Aerodynamic Vectoring

Zac Humes
Utah State University

PARTICLE CHARACTERIZATION AND CONCENTRATION USING AERODYNAMIC VECTORING

by

Zachary E. Humes

A thesis submitted in partial fulfillment
of the requirements for the degree

of

MASTER OF SCIENCE

in

Mechanical Engineering

Approved:

Dr. Barton L. Smith Major Professor	Dr. Robert Spall Committee Member
Dr. Lejun Li Committee Member	Dr. Byron R. Burnham Dean of Graduate Studies

UTAH STATE UNIVERSITY
Logan, Utah

2008

Abstract

Particle Characterization and Concentration Using Aerodynamic Vectoring

by

Zachary E. Humes, Master of Science

Utah State University, 2008

Major Professor: Dr. Barton L. Smith
Department: Mechanical and Aerospace Engineering

An experimental demonstration of a new, non-contact particle characterization technique called Aerodynamic Vectoring Particle Sorting (AVPS) is presented. AVPS uses secondary blowing and suction control flows–flows that are a fraction of the jet flow rate–to sharply change the direction of a planar, particle-laden jet. As the jet is vectored, particles present in the flow experience a resultant drag force, dependent upon their size, that balances inertia. Since this balance determines the particle's trajectory, vectoring the flow leads to a separation of particles downstream. This simple, low-pressure-drop sorting technique classifies particles with less risk of damage or contamination than currently available sorting devices.

AVPS is also shown to be capable of concentrating aerosols. Our measurements indicate that an air sample containing water-like particles can be concentrated by a factor of 10 using AVPS.

(60 pages)

To all of those who have asked me to fix everything from airplanes to computers.

Acknowledgments

Thanks to my patient and brilliant wife for helping me along the way, Terry Zollinger who built anything no matter how "impossible" and to Dr. Barton Smith for all of the opportunities to grow as a person and a professional.

Zachary E. Humes

Contents

Page

Abstract . . . . . **iii**

Acknowledgments . . . . . **v**

List of Figures . . . . . **vii**

1 Introduction **1**

2 Literature Review **4**
2.1 Jet Vectoring 4
2.2 Particle Classification 6
2.3 Aerosol Concentration 6

3 Objectives **8**
3.1 List of Objectives 8
3.1.1 Jet Vectoring 8
3.1.2 Particle Classification 8
3.1.3 Aerosol Concentration 8

4 Approach **9**
4.1 Experimental Setup and Measurements 9
4.1.1 Particle Image Velocimetry Measurements 12
4.1.2 Shadowgraphy Measurements 14
4.1.3 Concentrated Flow Measurements 15
4.2 Vectoring Schemes 19
4.3 Comparison to Coanda Jet Flow 20

5 Results **23**
5.1 Classification Results 23
5.2 Aerosol Concentration Results 27

6 Conclusions and Recommendations for Further Work **31**

References **32**

Appendix **34**

List of Figures

Figure Page

1.1 Schematic of AVPS using pure suction. 3

2.1 Oscillating flow facility used by Smith and Glezer. 5

4.1 AVPS facility. 10

4.2 Powder feeder or "fluidizer." 11

4.3 Fuji ring compressor. 12

4.4 The atomizer produces small seed particles for the PIV. 13

4.5 a) Camera images showing illuminated seed (inverted image). b) Velocity vectors produced using LaVision's software. 14

4.6 Sketch of shadowgraphy system utilized to calculate size and velocity of sorted powders. 15

4.7 Velocity profile of vectored primary jet flow and location on vectored field, parameters used to concentrate particles 0.6 times the density of water. . . 17

4.8 Velocity profile of vectored primary jet flow and location on vectored field, parameters used to concentrate particles 2.5 times the density of water. . . 17

4.9 OPC probe diameter optimized for greatest concentration ratio. 18

4.10 Probe used to sample the concentrated particle laden air. 18

4.11 Vectoring with suction and blowing (top row) and suction only (bottom row). A velocity vector map of each case is shown at the left. Turbulence Kinetic Energy for two primary jet speeds are shown in the center and right plots. . 20

4.12 Streamwise mean and fluctuation velocity profiles of the 90° vectoring case for (a) laminar (Re = 5000) and (b) turbulent (Re = 9000) conduit flow. Also included in the plots are data from Neuendorf and Wygnanski [23] (labeled NW) for Coanda flows and a wall jet. 22

5.1 Backlit photos of some of the particles used on our study. (a) Duke Scientific solid glass sphere. (b) 3M hollow glass microspheres. The smaller particles attached to the sphere are amorphous silica added to improve the flow of the product. (c) A second example of a 3M glass microsphere that appears to be solid. 23

5.2 A time exposure laser-sheet illuminated photograph of (a) $\gamma = 2.5$ and (b) $\gamma = 0.6$ glass spheres undergoing sorting by aerodynamic vectoring. 24

5.3 (a) Data are acquired in small windows two jet widths downstream. (b) The sorting result. Data points represent the mean particle diameter acquired at each location, while the error bars represent the standard deviation. 25

5.4 Grade Efficiency Curves (GEC) for sharpness of cut measurements. The numbers above the curves refer to the bin at which the measurement was made (Figure 5.3a). The solid lines represent $\gamma = 0.6$ particles from 3M. The dashed curve is a result for the $\gamma = 2.5$ Duke scientific particles at one location. 26

5.5 Optical Particle Counter (OPC) set on wall near blower for baseline reading of pre-concentrated material. 28

5.6 Room built to simulate a field measurement. 29

5.7 Fluidizer and fan used to introduce particles into ambient air. 29

5.8 Sketch showing the location that concentrated particles were collected. . . . 30

5.9 Air concentration of particles in the range $7 - 10\mu$m by AVPS showing an average concentration of a factor of 9.5. 30

Chapter 1

Introduction

In many powder-based industrial processes, it is desirable that the powder be comprised of particles of a relatively uniform size. However, most powder manufacturing processes are incapable of making uniform-sized particles. If a uniform size is necessary, classification of the particles by size is required [1].

An Aerodynamic Vectoring Particle Sorting (AVPS) design was studied to determine its effectiveness to classify and concentrate an aerosol. The classification performance of the AVPS device was measured using a particle sizing technique called Shadowgraphy. Two powders of differing specific gravities were tested for the classification study. One being constructed of solid borosilicate glass particles and the other of non-uniform hollow glass bubbles. This experiment was performed to further the study in aerosol classification with several industrial applications that could benefit from the characteristics of the AVPS. These applications include classification of: excipients (a lactose based carrier used in the manufacturing of pharmacueticles), active drug ingredients, metal powders, glass bubbles (used in deep sea insulation) and nutraceuticals.

Today, the common industrial techniques for particle size classification are screening/sieving, free vortex technology or "cyclones," and forced vortex technology or "air classifiers." Each of these separate particulate into "large" and "small" bins. For over a century particle classification has been accomplished through use of plate, and more recently, virtual impactors [2]. In either case, the main flow is subject to an angular acceleration which serves as the primary means for separating particles. The plate impactor accelerates the particle laden flow through a nozzle onto an impinging surface where the main flow turns parallel to the plate. Larger particles impact an adhesive surface while smaller particles remain in the flow. Torczynski and Rader [3] described some problems stemming from

these methods. Placing a plate in the flow path can cause contamination of physical or chemical properties. Also, impaction of particles on a surface may lead to fragmentation or agglomeration, or particles may be re-entrained into the main flow. Furthermore, pressure drops can be large for impact-based approaches which can limit transport rates, increase device size and pumping energy requirements.

If a range of particle sizes is to be collected, more simultaneous cuts are required and impactors are staged. A unique device called an "elbow jet" allows powder to be separated into three bins simultaneously [4]. This device uses a combination of a Coanda surface and a blowing control flow to modify the direction of the particle laden flow. While online configurable (by modification of the control flow rate), the elbow jet device is limited to three collection bins.

We present a new characterization method called Aerodynamic Vectoring Particle Sorting (AVPS). AVPS sorts particles by using small control flows to rapidly alter the path of a particle-laden jet, as shown in Figure 1.1.

The innovation of AVPS is the non-contact method by which the particle laden flow is vectored. The flow is turned through the action of small control flows near the exit plane. Particles of sufficient mass leave the jet flow and enter the slow-moving entrainment flow that results from the shear between the primary jet and the ambient gas. The particles are decelerated at a rate dependent on their size and can be collected by bins or, alternately, fed into further processes while still airborne. Meanwhile, very small particles follow the jet flow. As a result, multiple simultaneous sharp cuts can be made without device staging (and associated energy costs) or surface contact that often results in particle damage and agglomeration. The number of collection bins or process feeds is adaptable to process requirements.

Additionally, sorting is often used as a diagnostic tool to determine the number of particles of a given size in a sample. When detection of particles, such as pathogens, is required, it may be beneficial to concentrate a sample, which can be achieved using a sorting apparatus [5].

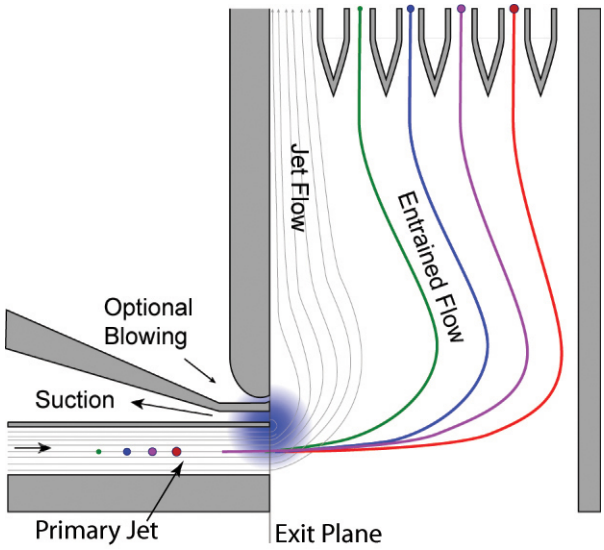

Fig. 1.1: Schematic of AVPS using pure suction.

The concentration of particles was investigated to further concentration of aerosols. Glass bubbles having a specific gravity close to that of water were used in the study. The Particle Size Distribution (PSD) and density were chosen to closely match common pathogens. The quantitative concentration factor was measured with Optical Particle Counters (OPC).

Chapter 2

Literature Review

2.1 Jet Vectoring

Numerical and experimental research was performed with both coanda surfaces and aerodynamic actuation. One study showed that reattachment of separated jet flows to adjacent solid surfaces can be enhanced by time-invariant suction. Jet vectoring was achieved using low-volume suction to induce counter-current flow between the edge of a rectangular Mach 2 primary jet and an external collar [6]. The counter-current flow led to increased mixing that in turn resulted in low pressure regions near the collar. A more recent study enhanced a jets tendency to attach to a nearby conical diffuser by introducing disturbances with synthetic jets [7, 8]. This scheme has now been extended to closed-loop control [9].

Another method was demonstrated numerically by Hammond and Redekopp [10] in a shear layer between parallel streams of different speeds. In their numerical investigation, Hammond and Redekopp used suction at the downstream end of the flow partition in a plane shear layer to effect vectoring toward the high-speed stream. For sufficiently large suction volume flow rates (suction speeds on the order of 20%-40% of the free-stream velocity), the global (absolute) instability of the flow partition wake was suppressed, and the low-speed fluid was vectored toward high-speed side. The authors also reported that the direction and extent of the vectoring can be altered by modifying the symmetry of the suction flow such that the shear layer is vectored toward the side from which the bulk of the suction flow is entrained. Vectoring with multiple suction and blowing slots was reported by Smith *et al.* [11]. These authors reported that this vectoring method was effective when an extended Coanda surface was present, but relatively ineffective without this surface. The interaction between a continuous primary jet and adjacent synthetic control jets in the absence of extended control surfaces was investigated experimentally by Smith and Glezer [12] and

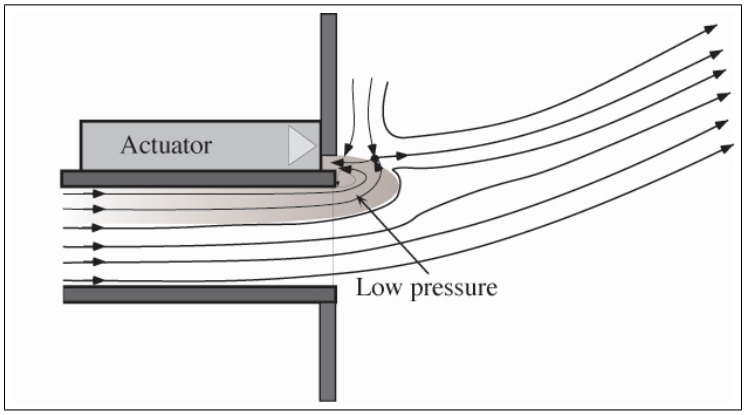

Fig. 2.1: Oscillating flow facility used by Smith and Glezer.

numerically by Guo *et al.* [13, 14]. In contrast to conventional continuous jets, synthetic jets can transfer linear momentum to the flow without net mass injection across the flow boundary. Synthetic jet actuation provides a localized combination of alternating blowing and suction through the same flow orifice. Due to the suction flow, the time-averaged static pressure near the exit plane of a synthetic jet is lower than the ambient pressure. The investigation by Smith and Glezer [12] showed that entrainment of primary jet fluid by an adjacent synthetic jet leads to alteration of the static pressure near the exit plane and results in deflection of the primary jet toward the synthetic jet as shown schematically in Figure 2.1. However, this form of actuation requires the development of actuators that can deliver oscillatory flow at a desired frequency and amplitude within the geometric constraints of a given flow apparatus. An important finding of that study was that for a fixed actuator input (frequency and amplitude), the vectoring force increased linearly with the primary jet Reynolds number up to a critical value Re_c. This critical Reynolds number was found to increase with the actuator frequency. Unfortunately, most interesting flows occur at higher Reynolds numbers.

Aerodynamic vectoring has been shown previously to be an effective method for sharply vectoring a jet [15]. It was later shown theoretically that particles placed in this flow could be sorted by size [16].

2.2 Particle Classification

Much research has been done on particle classification using the other techniques mentioned above. There is a myriad of literature for each of the different techniques. For those unfamiliar with the topic will find a broad overview and comparison of the different methods in Shapiro and Galperin [17]. The authors provide a description of the different techniques as well as some applications. It is noted that many of the devices used for classification are limited to selecting out large and small particle sizes and if multiple cuts are desired then a "daisy chain" of devices with different cut points is necessary. The result is a loss in efficiency with an increase in power requirements.

A description of classifier efficiency and its definition is found in chapter 11 section 2 of Allen [18]. The result from a classification process can be presented in many different ways. Some use the Particle Size Distribution (PSD) which depend on the accuracy of the cut. Others present results in the form of a grade efficiency curve. The grade efficiency curve represents the probability that a particle of a certain size could be found in the "fines" bin instead of the "courses" bin. The theoretical efficiency limit of a classifier would be if no "fines" could be found in the "courses" bin. This limit is represented as a virticle line on the grade efficiency curve. The slope of the line on the grade efficiency curve also provides a measure of the efficiency and is refered to as the cut sharpness or sharpness index.

2.3 Aerosol Concentration

Aerosol concentration has been experimentally studied as a means to decrease sample time for biological agent detection. Many of the studies are performed using virtual impactors due to the amount and availability of theoretical and experimental background information. They also have been used for the purpose of aerosol concentration for years.

An experimental study by Romay *et al.* [5] reports a 150-270 times concentration factor of particles between 2.3 to 8.4μm in aerodynamic diameter. One and two-stage virtual impactors were used in series to achieve the high concentration factors. However, when each stage is looked at individually only a concentration factor of 20 is reported for the first stage with a decline in efficiency to a factor of 15 for the two-stage section. We

will look at only one of the stages of the concentration device for the purposes of this paper because the AVPS could also be configured in series to increase the concentration factor with similar trade offs.

Another study by Kim *et al.* [19] evaluated the ability of multi-nozzle virtual impactors to concentrate an aerosol. The focus of that study was to determine the trade off between multiple nozzles and pressure drop. Having the nozzles be in parallel decreases the collection efficiency of the virtual impactor. It was noted that the concentration factor achieved was about a factor of 16 which is in close agreement with Romay *et al.* [5].

Chapter 3

Objectives

3.1 List of Objectives

The primary objectives completed for this study include:

3.1.1 Jet Vectoring

- Determine best vectoring configuration for sorting glass powder.
- Compare with Coanda surface vectoring.
- Analyse the turbulence levels for different configurations.

3.1.2 Particle Classification

- Sort two glass powder types of differing specific gravity.
- Measure the accuracy of sorting using Shadowgraphy.
- Produce a grade efficiency curve for each powder.

3.1.3 Aerosol Concentration

- Modify facility to allow for aerosol concentration.
- Concentrate particles similar to common pathogens.
- Determine the amount of concentration provided by the AVPS unit.

Chapter 4

Approach

4.1 Experimental Setup and Measurements

The demonstration facility is shown schematically in Figure 4.1 while the drawings are provided in the Appendix. This is the configuration used for classification measurements. The primary jet in the facility is oriented flowing downward. (Note that in all other figures, the jet is shown flowing horizontally.) Particulate was loaded into the hopper of a powder feeder, or "fluidizer" shown in Figure 4.2. The fludizer was designed to improve the fluidization of powders at low flow rates. The fluidizer incorporated a vibrating feeder in an airtight tank possessing an inlet for a carrier gas (compressed air for the present study) and an outlet for the carrier gas and the particulate. The carrier gas entered the tank causing a slight pressure increase. This pressure difference drove the flow through a funnel that received the particulate from the vibrating feeder and mixed the particulate into the carrier gas. The flow of air through the fluidizer was controlled with a rotometer (not shown). Concentrated particulate was delivered to the AVPS facility through a stainless steel tube connected to the funnel, which was grounded to limit static charge. The tube introduced particles into the rectangular channel (1) located at the top of the contraction. The velocity of this flow matched the clean air velocity at the channel exit (which was before the contraction) to limit mixing due to shear. The requirement for matched flow velocities formed the basis for the limit on particle throughput. The fluidizer used in the experimental setup required a particular flow rate for the carrier gas, therefore, if the feedrate of the powder was increased there was also an increase in flowrate for the carrier gas. The particle channel terminated at the start of the contraction (2).

The flow outside the particle channel is clean air supplied by a main, frequency-controlled, blower. The contraction (3) served to damp out disturbances generated by

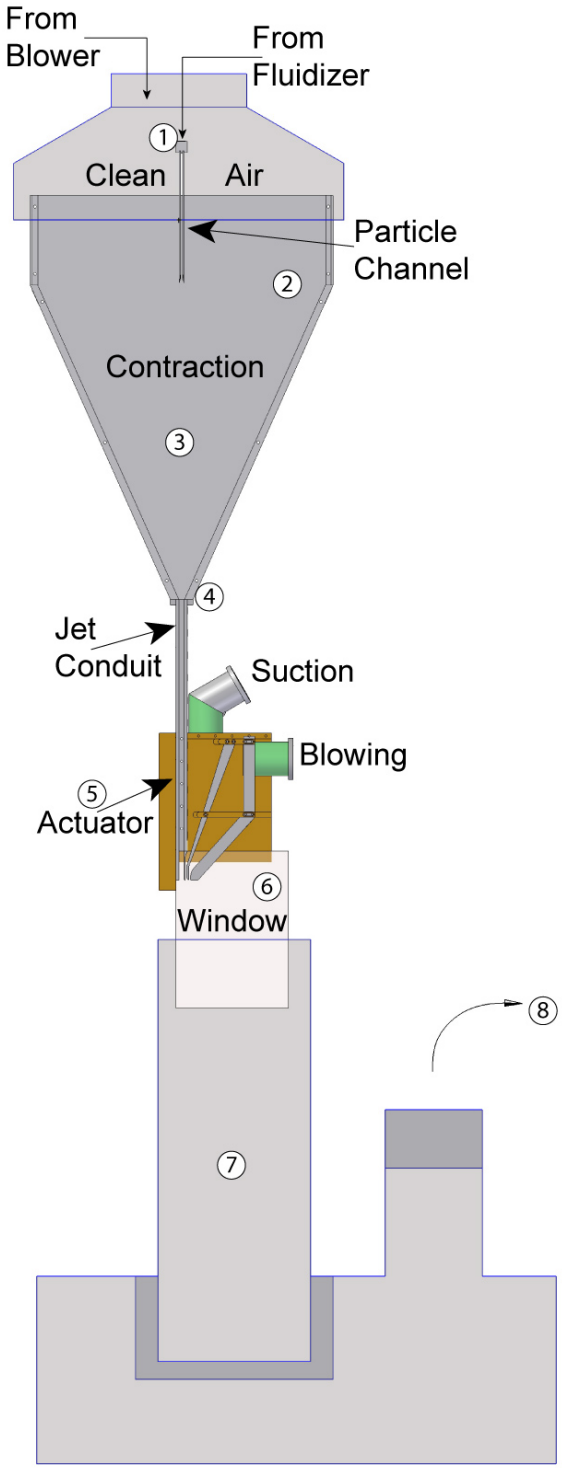

Fig. 4.1: AVPS facility.

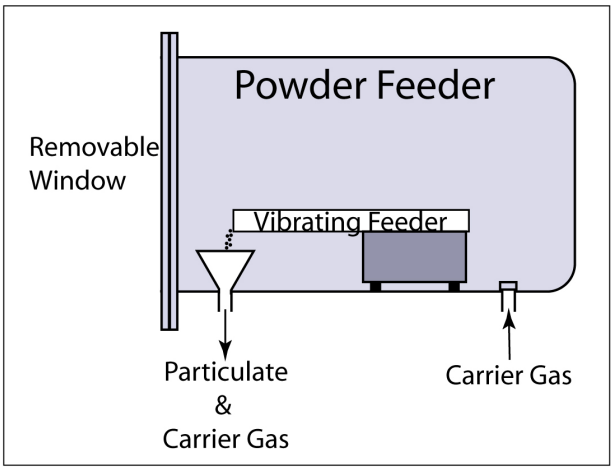

Fig. 4.2: Powder feeder or "fluidizer."

the particle channel and helped maintain steady, laminar flow at the exit. The jet conduit (4) started at the termination of the contraction. The inner surfaces of the conduit were polished to reduce disturbances.

Jacketing the particle flow inside layers of clean air required that the particulate be introduced to the flow stream without generating disturbances that may lead to flow fluctuations and decreased accuracy. In order to minimize disturbances, the particulate was distributed across the entire span of the sorter before flowing through a long channel (labeled 1 in Figure 4.1). The channel length allows time for disturbances generated in the injection process to be damped out before entering the clean air flow. Considerable care was taken to eliminate shear between the clean and particulate flow by ensuring that the flow speed out of the channel is identical to the clean air flow. This was done using a hot film probe located a short distance down stream of the particle channel to detect vortices formed by shear layer instabilities. A LabView program was developed which allowed for the realtime monitoring of the fluctuation levels as well as perform an FFT to easily identify the fluctuation frequencies. To further reduce disturbances generated in this process, the

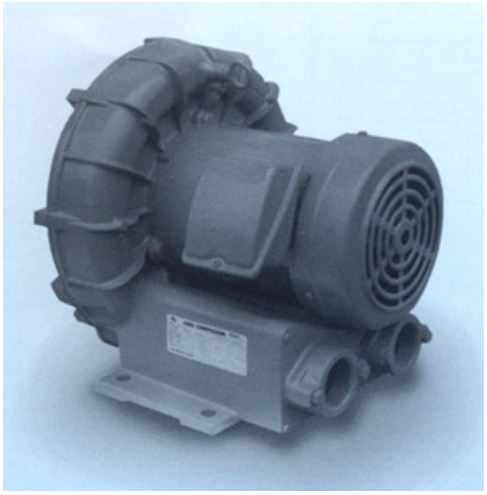

Fig. 4.3: Fuji ring compressor.

combined flow entered a long contraction which damped fluctuations and further reduced the particle sheet thickness. The smaller sheet lead to higher accuracies, since the origin of the particles more closely resembled a single point.

The actuator was built onto the end of the jet conduit (5). The actuator consisted of two small adjacent flow control slots, one for blowing and a second for suction. The suction slot was closest to the primary jet. Flow through these slots was provided by a frequency-controlled ring compressor Figure 4.3.

After leaving the jet conduit, the flow was constrained in the spanwise direction by two transparent windows (6) which made optical measurements possible. A large pipe (7) sat downstream of the actuator. A small flow was drawn through this pipe by a secondary blower, and particulate was removed from the room by a HEPA filter (8) after all measurements were made.

4.1.1 Particle Image Velocimetry Measurements

Velocity field measurements were made using a Particle Image Velocimetry (PIV) system by LaVision Inc. consisting of a 12-bit 1.3-Megapixel (1280×1040) camera, a pair of 50 mJ Nd:YAG lasers with sheet optics, and an acquisition PC including a frame grabber and a timing board. A fluorescent rhodamine based paint was applied to all surfaces to shift

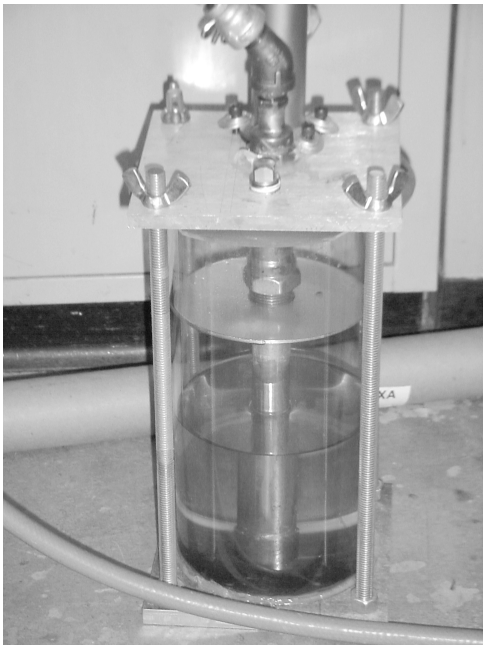

Fig. 4.4: The atomizer produces small seed particles for the PIV.

laser reflections to wavelengths that were removed by a filter on the camera optics. The laser sheet entered the facility from one cross-stream side while terminating on a barrier. The sheet was placed between the spanwise centerline ($z = 0$) and the spanwise wall as a compromise between our desire to obtain 2-D mean data and to minimize the extent of the region near the exit surface that cannot be observed due to parallax.

Olive oil droplets formed by a Laskin nozzle apparatus (built in house) were used as seeding particles or tracer particles. These tracer particles should be sufficiently small to follow the flow exactly and reflect enough laser light. Olive oil droplets formed by an atomizer have been suggested as an appropriate tracers (aka seed). To build the atomizer, several very small holes were drilled toward the bottom of a copper pipe placed in olive oil. Above the oil level, a baffle plate was used to capture the droplets of oil too large for the PIV. Smaller particles moved past the baffle plate, through the flow conditioners, and out the actuator with the flow. The atomizer used is shown in Figure 4.4.

The laser light illuminated the seed, which were much brighter than the background. Groups of these bright spots were analysed by a software algorithm called cross-correlation

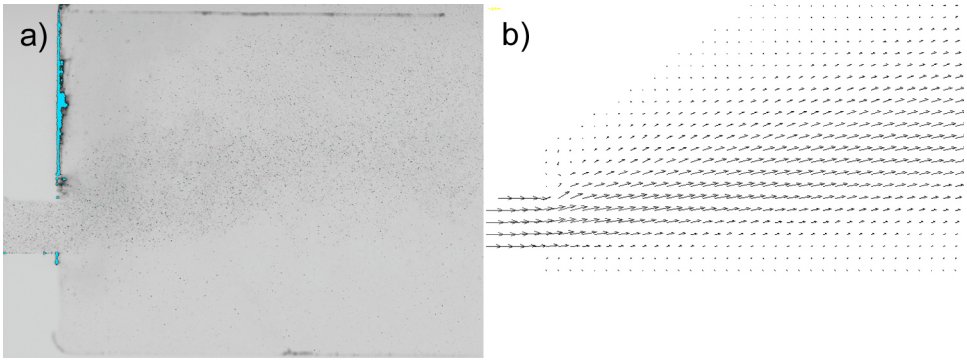

Fig. 4.5: a) Camera images showing illuminated seed (inverted image). b) Velocity vectors produced using LaVision's software.

developed by LaVision to produce velocity vectors. An example of raw picture data and processed vectors are shown in Figure 4.5. The picture showing the seed has been inverted, so the background is white and the seed is dark. After the raw data was taken and processed with software from LaVision, additional codes were written to compute other quantities of interest.

The droplets produced were estimated to be 1-2 μm in diameter. The droplets were drawn into the facility at the inlet. Care was taken to ensure that the images of the droplets on the Charge Coupled Device (CCD) array were somewhat larger than 2 pixels to eliminate pixel locking while providing maximum accuracy [20]. Multiple cross-correlation passes with a final interrogation-region size of sixteen pixels were used.

4.1.2 Shadowgraphy Measurements

Particle trajectory/size measurements were made using a LaVision shadowgraphy system based on a 45 mJ Nd:YLF laser (represented by (1) in Figure 4.6) coaxially aligned with a 1.0 megapixel 10-bit high speed camera capable of 3000 Hz recording rate (5). A diffuser was placed on the laser providing a uniformly-illuminated background (2). Shadows of particles (3) were cast onto the camera sensor through microscope optics (4) placed on the camera. Software provided by LaVision detected in-focus particles and determined their size based on a calibration performed earlier (6).

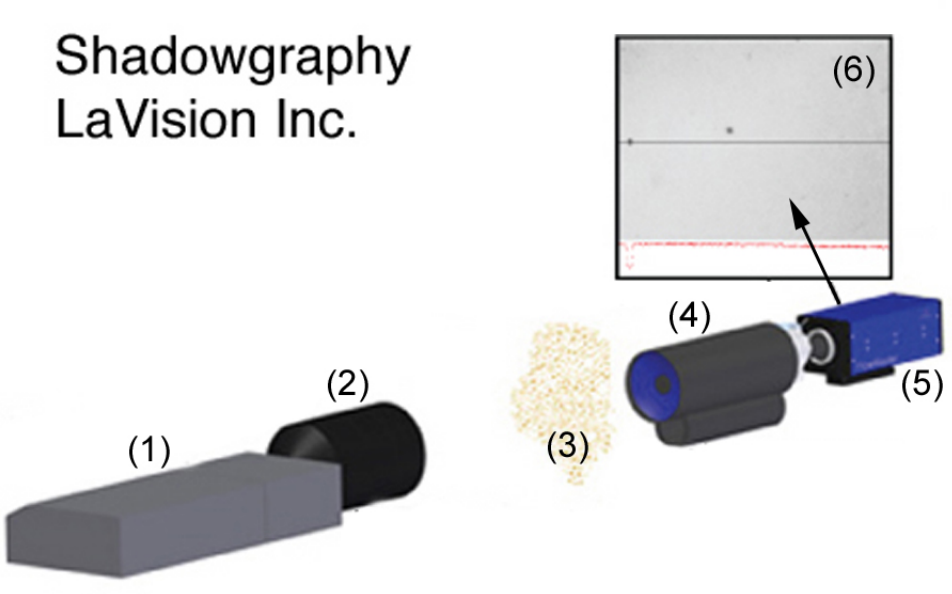

Fig. 4.6: Sketch of shadowgraphy system utilized to calculate size and velocity of sorted powders.

For these measurements, the field of view was 733 μm by 733 μm resulting in a pixel resolution of 1.4 μm. According to Nishino *et al.* [21], the accuracy of this measurement is $\pm$ 4 μm for a particle distribution of 10-500 μm and for particles smaller than 10 μm the accuracy diminishes. However the pixel resolution used by [21] was 6.8 μm, possibly causing the accuracy to be less for particles smaller than 10 μm.

4.1.3 Concentrated Flow Measurements

Sampling of the concentrated flow was performed with a Met One Optical Particle Counter (OPC). The accuracy of the sensors is 2% of reading. The OPC draws a small-volume sample (in this case, 0.3 L/min). A laser illuminates each particle in the aerosol and a photo detector measures the amount of light diffracted and refracted. The number of particles and their size, which is calculated by light intensity, is recorded at sample intervals. The OPC breaks the distribution into bins that can be chosen by the user. The bins chosen for this study in microns were 0.3-1, 1-2, 2-3, 3-4, 5-7, and 7-10. Before any measurements were taken, a benchmark test was performed to ensure a matching reading for both OPCs.

Probes were manufactured to be installed on the OPCs to decrease the cross sectional

area through which the particles were collected. This allowed for the narrowing of the Particle Size Distribution (PSD) sampled by the OPC. Care was taken to avoid a difference in the probe entrance and entrainment flow velocities. The velocity profiles were extracted from the PIV data for the entrainment flow (which is slower than the jet flow) and are shown in Figures 4.7 and 4.8. The entrainment velocity was matched with the inlet velocity of the probe based on the OPC's factory calibration stating 0.3 L/min. This provided a good first estimate of the probe diameter needed to reduce velocity discrepancies before and after the probe opening. Fine tuning of the optimal probe size was done by fixing the location of the probe and flow parameters while changing the probe diameter. The ratio of the concentration to baseline sensors was used to determine maximum signal or optimal probe diameter which is shown in Figure 4.9. The particles were not jacketed for the concentration study which produced an optimal location in the downstream flow where particle paths were not crossing as much. To find this location the probe shown in Figure 4.10 was traversed in the y-direction while holding all other parameters constant until the maximum signal was found. The end of the probe was also sharpened to decrease the stagnation flow along the rim of the probe. Unsteadiness and pressure drop inside the probe were reduced by using a very gradual 7° slope in the expansion which is widely accepted to impede flow separation leading to pressure drop and mixing. Mixing could cause the particulate to be deposited on the side of the inlet and later be released in a large quantity causing the measurement to be less consistent.

A Labview program was developed to return the values recorded by the OPC in real time. The program also calculated the ratio between the reference and concentration probes, mean, and standard deviation. This was crucial in determining the optimal location of the probe for maximum signal. Along with being able to see when the vectoring would turn on, the effects of any parameter change such as probe location or flow rates could be instantly detected.

The flow ratios of the primary jet and suction flows were measured using hot film anemometry. The primary jet velocity was calibrated against the static pressure of the

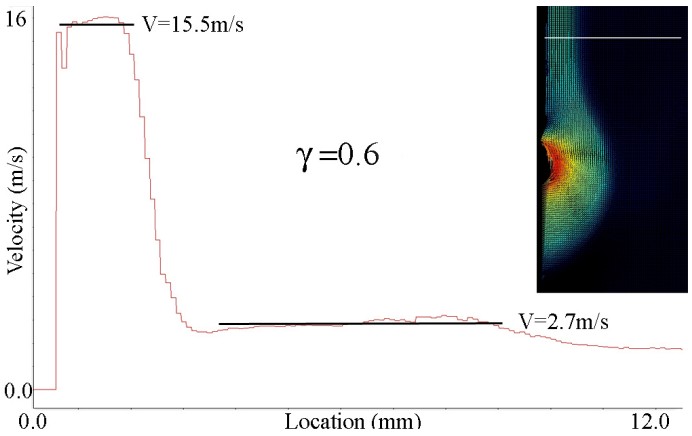

Fig. 4.7: Velocity profile of vectored primary jet flow and location on vectored field, parameters used to concentrate particles 0.6 times the density of water.

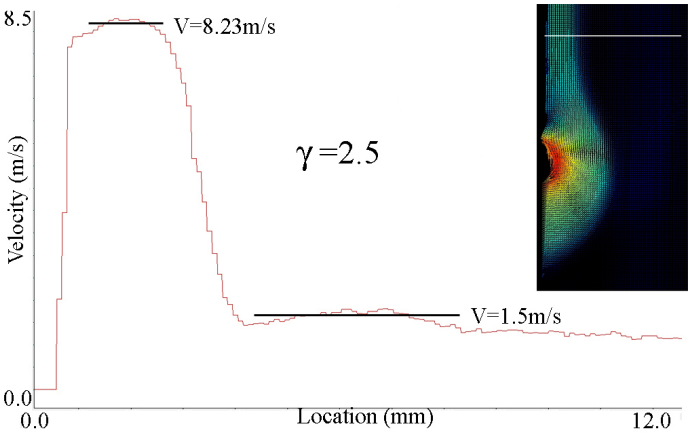

Fig. 4.8: Velocity profile of vectored primary jet flow and location on vectored field, parameters used to concentrate particles 2.5 times the density of water.

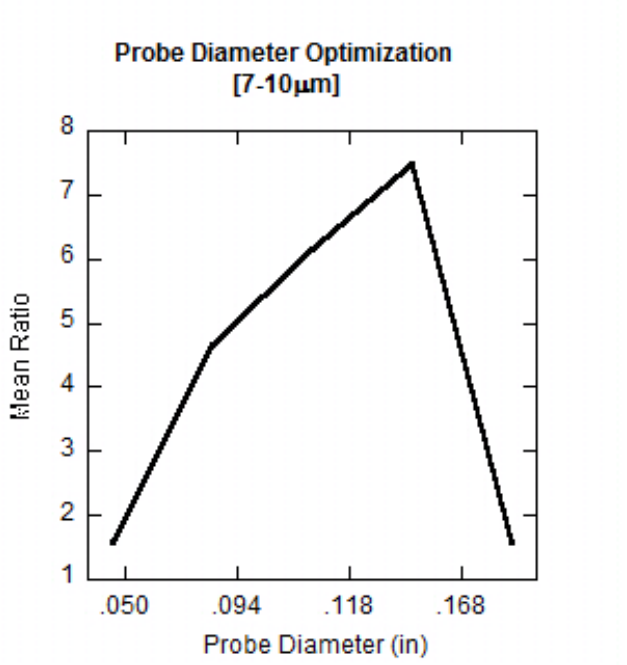

Fig. 4.9: OPC probe diameter optimized for greatest concentration ratio.

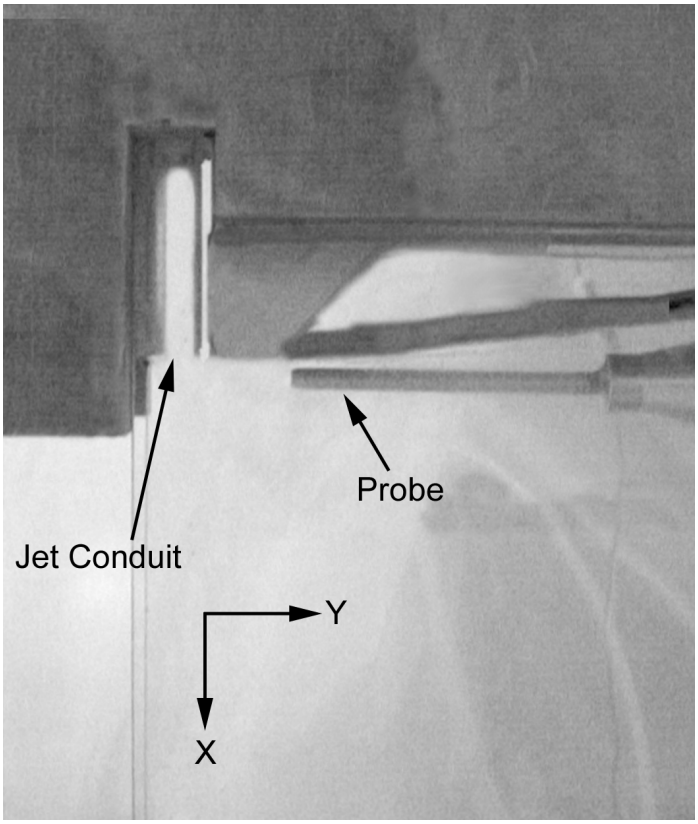

Fig. 4.10: Probe used to sample the concentrated particle laden air.

primary jet and the calibration was used during the experiment, while the suction flow rate was monitored directly during the study using an in house built hotwire flow meter calibrated against a (LFE) Laminar Flow Element each time.

4.2 Vectoring Schemes

Before the sorting performance was investigated, the jet vectoring process was optimized for angle and stability. Although aerodynamic vectoring was optimized for mean vector angle with minimum control flow in earlier work [15], the earlier study did not consider the steadiness of the vectored flow. We have found the sorting accuracy to be sensitive to flow disturbances. Such disturbances are evaluated by examining the Turbulence Kinetic Energy (TKE) of the vectored flow. TKE is defined as the sum of the velocity fluctuations in each direction ($TKE = 3/4(u_{rms}^2 + v_{rms}^2)/U^2$).

There are two main causes of velocity fluctuations: turbulence and shear instabilities. Turbulence was eliminated by maintaining a low Reynolds number and laminar flow in the jet conduit. Shear flow may generate instabilities leading to fluctuations in two main locations: the shear layers of the primary jet (the regions where the flow speed is very different from the ambient), especially on the side away from the actuator, and in between the blowing flow and the primary jet. Shear layer instabilities in the primary jet have been minimized through the use of the relatively long jet conduit, which results in thick jet boundary layers and lower shear.

In Figure 4.11, two vectoring schemes are compared. The first scheme (top row) uses low control flow rates (10% of the primary) of blowing and suction, similar to [15]. The vector angle is larger than [15] because the blowing slot is angled upward. Unfortunately, shear effects are clearly visible between the primary jet and the blowing flow in the TKE plots. Furthermore, significant fluctuations are present in the lower edge of the jet of the higher-speed case. This result is due to high shear in the region between the fast-moving jet and the slow-moving ambient air. The second scheme (bottom row) uses a larger suction flow rate (30% of the primary) and no blowing. Interestingly, this pure suction case has no discernible shear layer instabilities at either speed. This result, in addition to the elimination

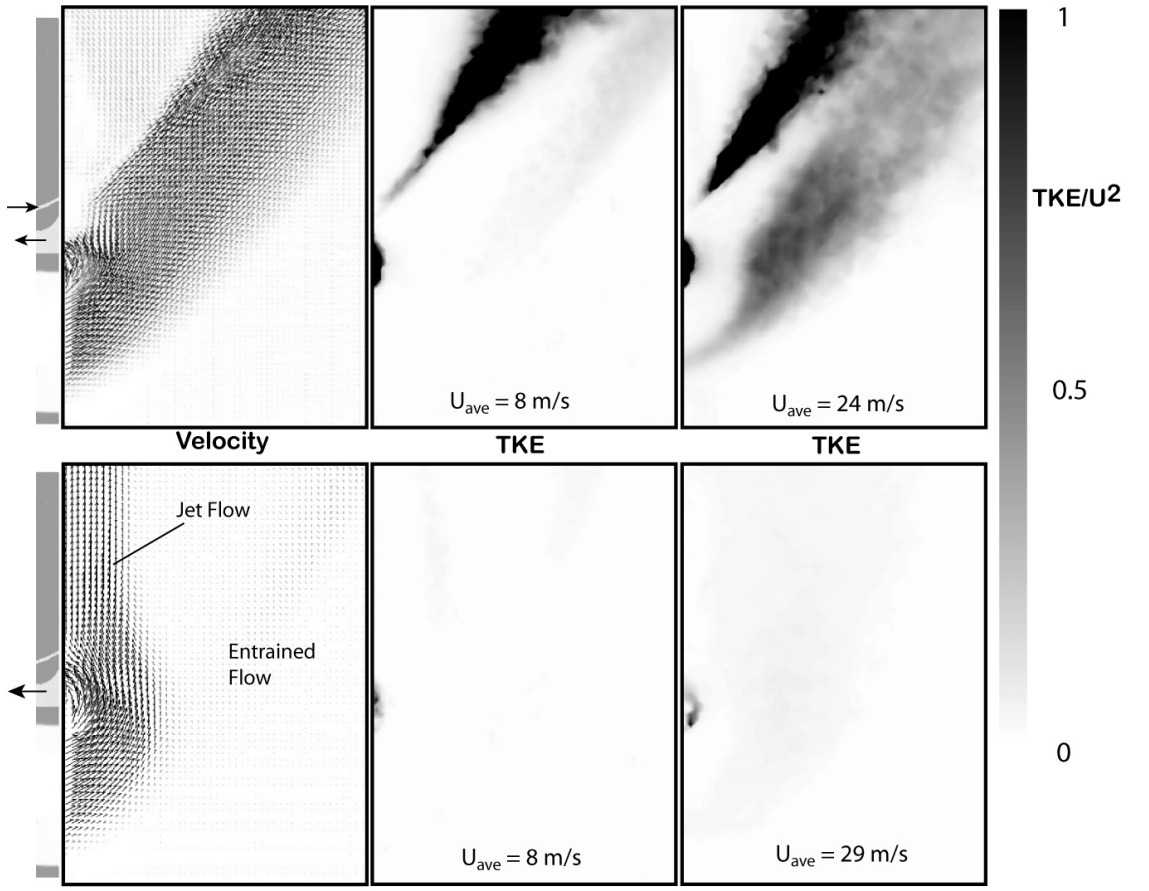

Fig. 4.11: Vectoring with suction and blowing (top row) and suction only (bottom row). A velocity vector map of each case is shown at the left. Turbulence Kinetic Energy for two primary jet speeds are shown in the center and right plots.

of the high fluctuations generated by the blowing slot and larger achievable vector angles (90°), makes the pure suction scheme preferable in spite of the increased suction flow rate. Due to the higher vector angle achieved and reduced TKE, the suction only scheme has advantage since particles leaving the jet flow are decelerated and collected in a region of low flow disturbance.

4.3 Comparison to Coanda Jet Flow

Another method to vector the jet flow that may initially seem similar is to use the Coanda effect [22]. The turning radius that is possible using Coanda is larger that that generated in the present scheme (typically much larger than the jet width). Furthermore,

vectoring with the Coanda effect amplifies disturbances in the flow, which, as discussed above, will have a detrimental effect on sorting accuracy. To illustrate this point, velocity fluctuations from the AVPS setup undergoing vectoring with suction only are compared to Coanda-jet results from [23] in Figure 4.12. Care must be taken to make a comparison to the Coanda flow, where a solid surface and the associated no-slip boundary condition is present. For the present flow, such a no-slip condition does exist on the upper surface of the jet conduit, and, as can be seen in the profiles, after turning 90°, the velocity of the fluid coming from this region is nearly zero, and this is used to estimate an effective turning radius and align these profiles with those of [23]. The velocities are normalized using the local variables of maximum velocity and jet half-width. Note that while the turning radius is much smaller for the present study ($R/H = 0.07$, where R is the effective cylinder diameter, while in [23], $R/H = 43.4$), the profiles have a similar shape. It is concluded in [23] that the profile shape does not depart significantly from that of a wall jet over this range of turning angles. A major difference between these flows can be seen in the streamwise fluctuations. We note that while the data at 0° and 90° are both labeled as u_{rms}, these are fluctuations in the local direction of the flow. For the aerodynamically-vectored flow, the fluctuation levels are small and do not grow due to turning. For the Coanda jets, the levels are much higher and generally increase with turning angle.

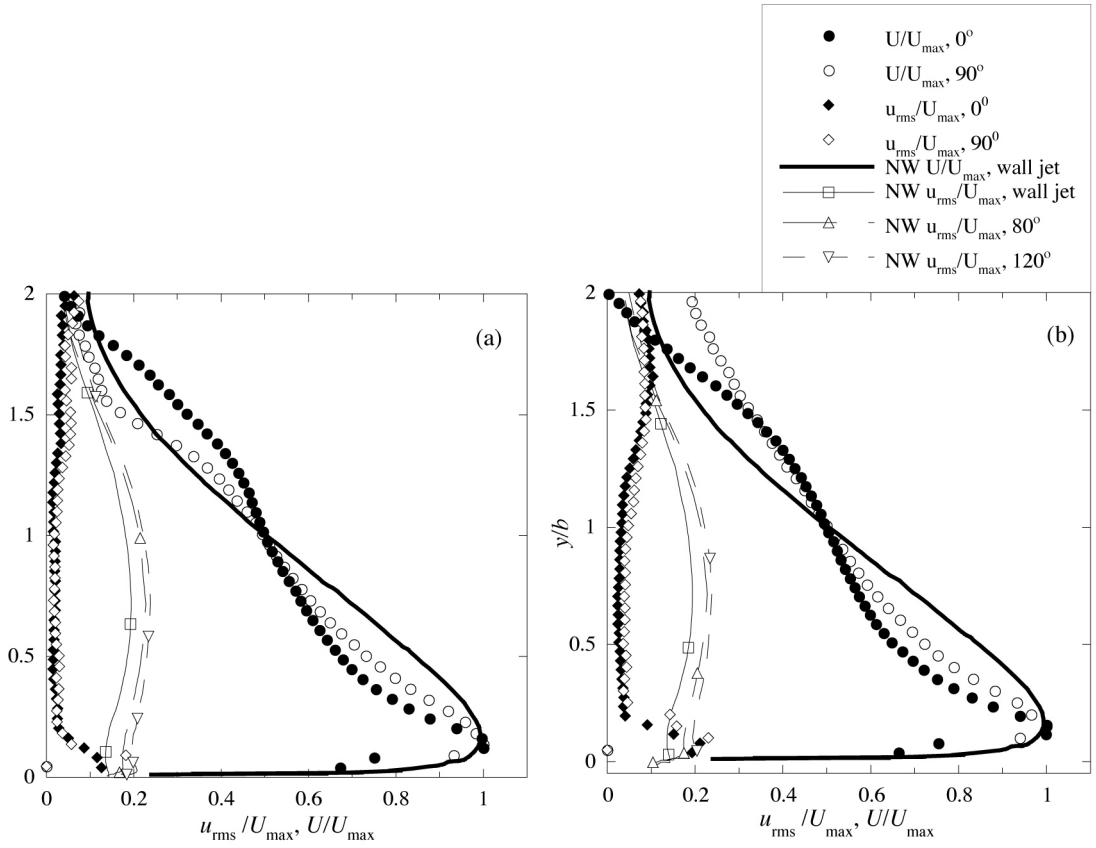

Fig. 4.12: Streamwise mean and fluctuation velocity profiles of the 90° vectoring case for (a) laminar (Re = 5000) and (b) turbulent (Re = 9000) conduit flow. Also included in the plots are data from Neuendorf and Wygnanski [23] (labeled NW) for Coanda flows and a wall jet.

Chapter 5

Results

5.1 Classification Results

Our first tests used laboratory-grade spherical glass particles with uniform density and spherical shape. These particles, produced by Duke Scientific (part number 424) have a specific gravity $\gamma = 2.5$, where γ is the ratio of the particle density to that of water. An image of an airborne Duke particle is shown in Figure 5.1a. Calibrated images such as this one are used to determine the diameter of the particle in our shadowgraphy system.

Our second series of measurements used industrial hollow glass microspheres (3M part number S60HS). Images of two of these particles are shown in Figure 5.1b-c. Since these particles do not flow as well as the Duke product, amorphous silica was added to improve our ability to fluidize the powder. Small amorphous silica particles can be seen clinging to the glass. Based on the images, it can be seen that the bubbles are not uniform in their construction. Specifically, it appears that the wall thickness varies resulting in a variation in the particle density. We note that this non-uniformity is not important to their intended application and is a common property of the material.

A still photograph of $\gamma = 2.5$ particles undergoing sorting is shown in Figure 5.2a. Several features of this flow are noteworthy. The jet is undergoing 90° vectoring with suction only. First, note that the particulate stream is "jacketed," or enclosed inside layers

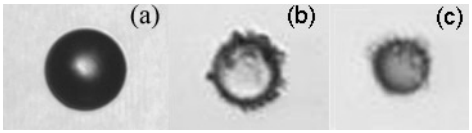

Fig. 5.1: Backlit photos of some of the particles used on our study. (a) Duke Scientific solid glass sphere. (b) 3M hollow glass microspheres. The smaller particles attached to the sphere are amorphous silica added to improve the flow of the product. (c) A second example of a 3M glass microsphere that appears to be solid.

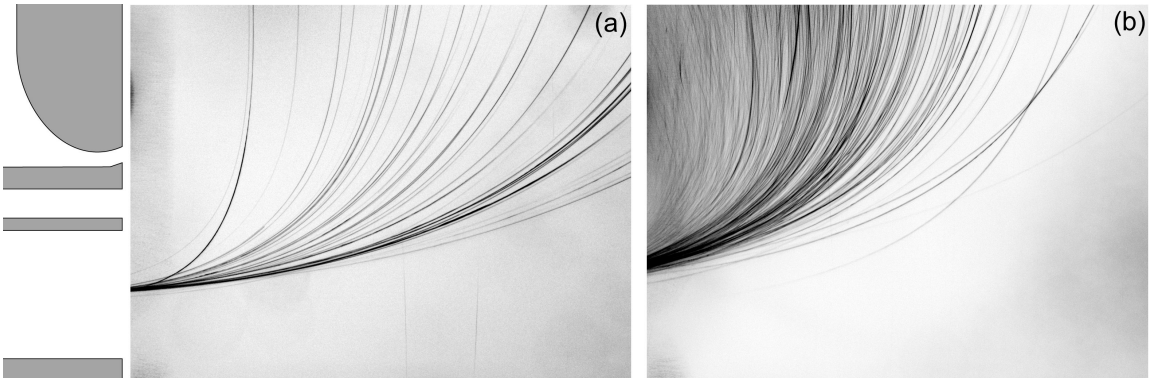

Fig. 5.2: A time exposure laser-sheet illuminated photograph of (a) $\gamma = 2.5$ and (b) $\gamma = 0.6$ glass spheres undergoing sorting by aerodynamic vectoring.

of clean air. This technique, which is standard in other sorting methods, serves to limit bias errors. The drawback of this method is that it limits the particle flow rate.

The majority of the particles (and all of the larger ones) quickly leave the jet flow and enter the slowly moving entrainment region outside the jet. As a result, the drag forces on the particles increase and they are decelerated substantially. Drag balances the inertia of the particles, resulting in a trajectory that is a strong function of particle diameter. All very small particles remain in the jet flow and exit on the top left. Particles of sufficient size will leave the flow without modifying their trajectory significantly. A similar photograph of the 3M particles being sorted is shown in Figure 5.2b. This feed material contained many more small particles than the Duke material. To sort the lighter 3M particles, the flow speed of the jet needed to be roughly double that for the heavier particles, consistent with the findings in [16].

This sorting effect is quantified using shadowgraphy techniques by measuring the size of particles passing through a series of small windows downstream of the actuator. Data are acquired on an arc two jet widths downstream of the exit, as shown in Figure 5.3a. Both types of particles were measured. For the heavier particles, the system was run with a flow speed of 8 m/s, while the lighter particles were sorted with a flow speed of 16 m/s. The data in Figure 5.3b shows the mean particle diameter measured at each location. The error bars indicate the standard deviation of the diameter of the measured particles. Data

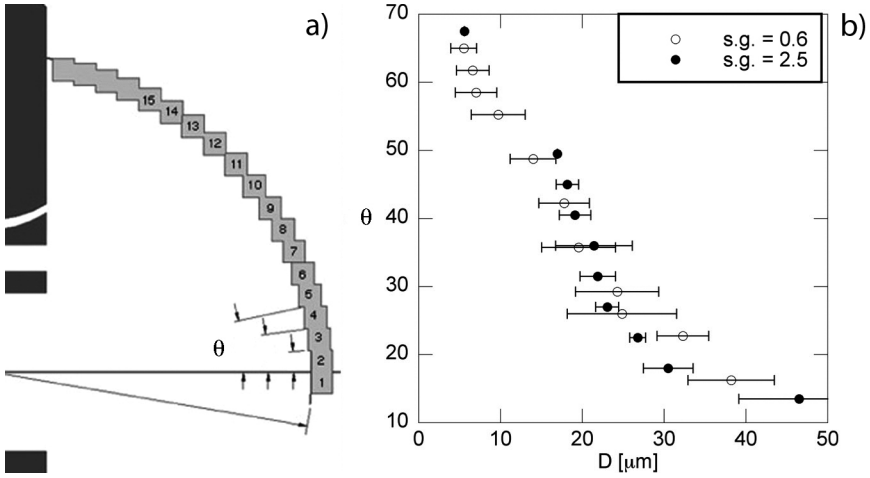

Fig. 5.3: (a) Data are acquired in small windows two jet widths downstream. (b) The sorting result. Data points represent the mean particle diameter acquired at each location, while the error bars represent the standard deviation.

points without error bars indicate that the sample size was too small for computation of a standard deviation.

Several general trends are apparent in the data. The ability to accurately sort is clear for all but the smallest angles, with the standard deviation for the $\gamma = 2.5$ particles dropping below 2μm for most locations. This is on the order of the uncertainty of our measurement technique (shadowgraphy). For the $\gamma = 2.5$ particles, the sample sizes at locations with particles smaller than 20μm are small due to a lack of particles of this size in the initial sample and due to shadowgraphy's low data rate. A single sample was acquired at two locations, and no standard deviation is computed there. The manufacturer of the material (Duke Scientific) claims a range of particle sizes from $5 - 50\mu$m. We measured the mean to be 35μm with very few particles below 20μm.

The lighter ($\gamma = 0.6$) particles from 3M have an initial distribution more suited the configuration of our demonstration device (i.e. there are larger number of smaller particles in the unsorted material). The measurements of these particles generally have larger standard deviations. There are two possible reasons for this. The first is that their smaller inertia makes these particles more susceptible to random ambient air fluctuations. However, the decrease in accuracy for the 3M particles as compared to the Duke particles is more likely

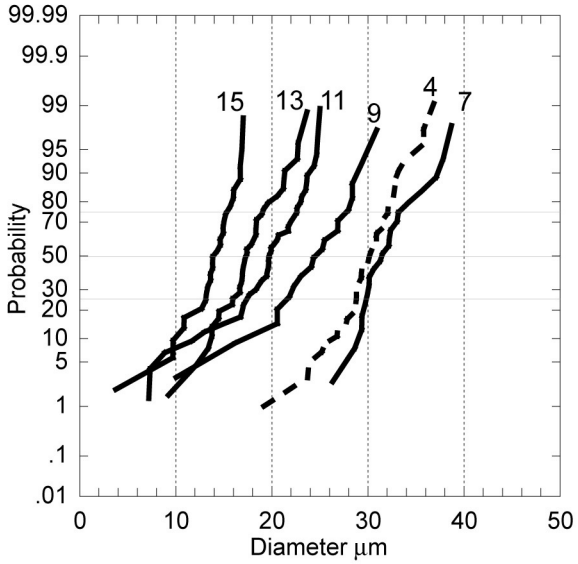

Fig. 5.4: Grade Efficiency Curves (GEC) for sharpness of cut measurements. The numbers above the curves refer to the bin at which the measurement was made (Figure 5.3a). The solid lines represent $\gamma = 0.6$ particles from 3M. The dashed curve is a result for the $\gamma = 2.5$ Duke scientific particles at one location.

due to density variations of the 3M particles. We have found many examples of thick-walled particles arriving at locations having mean diameters larger than their own. This is consistent with the particles having an above-average density. For instance, the particle in Figure 5.1b is typical, and was acquired at a location where the mean diameter was found to be 41μm. The particle in Figure 5.1c was acquired at the same location, but has a much smaller diameter. It also appears to be at least nearly solid. Many similar examples are included in this data set.

Particles in the range $40 - 50\mu$m are too heavy to sort with this flow speed, as their trajectories are all relatively straight. As a result, particles of many different large sizes arrive at angles below 20° resulting in a large standard deviation. Decreasing the flow speed would move these particles into the sortable range. Since we are operating at the lower flow limit of our current fluidizer, this change was not possible with our demonstration unit.

Sorting accuracy is more typically quantified in industry using cut sharpness. Cut sharpness is normally applied to classification processes where the particulate is divided

into “coarse” and “fine” bins. The sharpness is determined by examining the percentage of particles of any size entering the coarse bin divided by all particles of this size in the feed. A plot of this “Size Selectivity” as a function of particle diameter is called a “Grade Efficiency Curve.” This is the same as a typical probability plot, such as Figure 5.4. The x axis on this plot is particle diameter, while the y axis is the probability that any given particle is smaller than that value. The median diameter in a sample, D_{50}, is at 50%. Sharpness of cut is defined as D_{25}/D_{75}. High cut sharpness (good performance) is indicated by relatively vertical lines between the 25% and 75% probabilities. For the ideal but unattainable case, the cut sharpness is 1. The presorted cut sharpness of the 3M particles was measured to be 0.36, while for the Duke particles it was 0.56. This measure requires much larger sample numbers than standard deviation, so results are presented only for locations with sufficient data. Most of these are for the $\gamma = 0.6$ particles. Each line represents one of the data points in Figure 5.3. The cut sharpness for AVPS ranges from 0.8 for the lighter material to 0.9 for the heavier material. It is important to note that unlike other classifiers, AVPS is capable of making multiple cuts simultaneously.

5.2 Aerosol Concentration Results

The AVPS device can also be used to concentrate selected particle size ranges in air upstream of a sensor, such as a pathogen detector. The sorting facility first required modification. Removal of particle channel labeled (2) in Figure 4.1 and the installation of 1/4 inch cell honeycomb was necessary to allow for unobstructed flow of the particles (torturous-path elements such as foam tend to collect particulate). Particles were injected and mixed into ambient air. The mixed air was sampled by an Optical Particle Counter (OPC) located on the wall of the test area to provide a baseline particle count Figure 5.5. The AVPS blower inlet was open to the particle-laden ambient air causing both ambient and sorter air to have the same particle count. A second OPC was located at the jet exit to sample the concentrated air sample shown in Figure 5.8.

The OPC provides particle counts in various size ranges of the user’s choosing. Glass bubble particles with a similar density to water were used to simulate common pathogens.

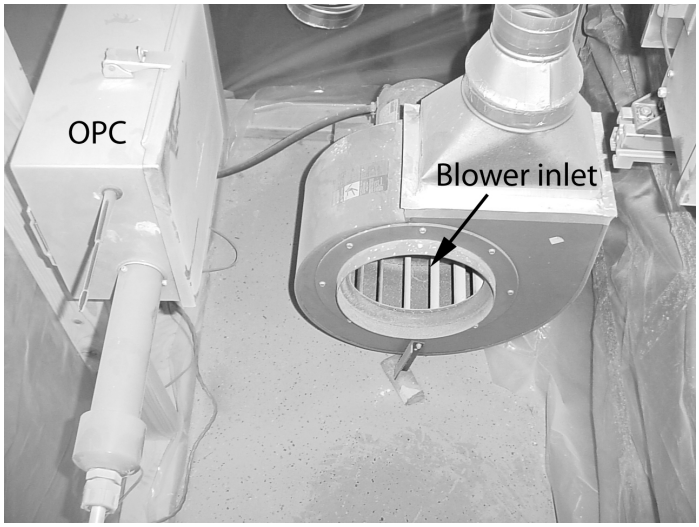

Fig. 5.5: Optical Particle Counter (OPC) set on wall near blower for baseline reading of pre-concentrated material.

An enclosure large enough to simulate a field measurement was constructed to allow for the ambient air to be laden with particulate before entering the concentrator (Figure 5.6). The particles were thoroughly mixed into the ambient air using a fan positioned at the exit of the fluidizer shown in Figure 5.7.

The flow ratios of the primary jet and suction flows were measured in the same way as described in §4.1.3.

A 0.94 inch diameter probe was placed 4.2 mm in the x-direction and 2.9 mm in the y-direction from the top of the primary jet exit. The ratio of suction flow to primary flow was 0.31 during the tests and the primary jet velocity was 15 m/s. The number of particles in the range $7 - 10\mu$m in the baseline and concentrated OPCs is shown in Figure 5.9. The ratio of these two measurements is the extent to which the sample has been concentrated, which in this case is nearly 10. Concentration factors of 3.5, 4.2 and 5.3 were achieved for 0.3-3, 3-4 and 5-7 microns, respectively.

Fig. 5.6: Room built to simulate a field measurement.

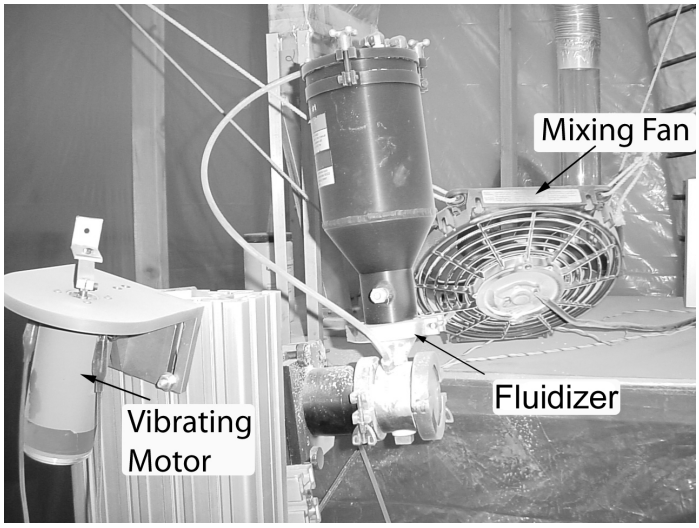

Fig. 5.7: Fluidizer and fan used to introduce particles into ambient air.

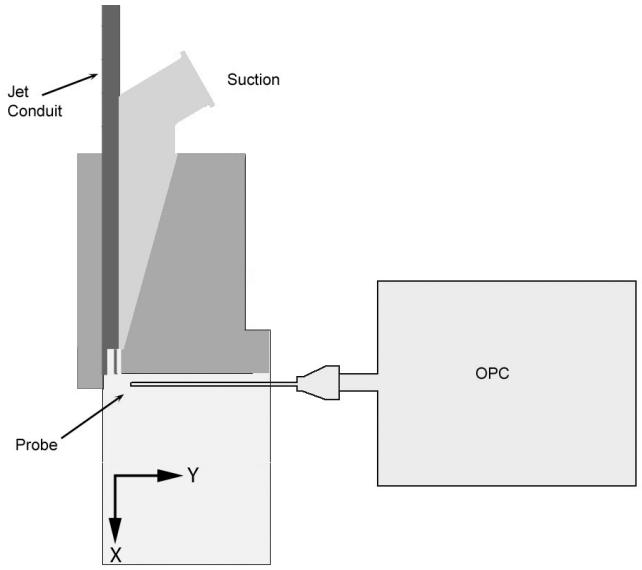

Fig. 5.8: Sketch showing the location that concentrated particles were collected.

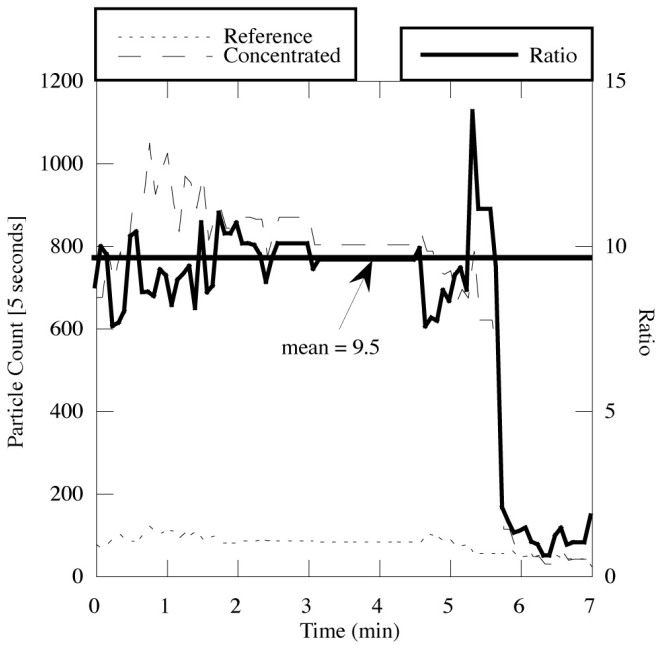

Fig. 5.9: Air concentration of particles in the range $7 - 10\mu$m by AVPS showing an average concentration of a factor of 9.5.

Chapter 6

Conclusions and Recommendations for Further Work

An aerodynamic vectoring actuator using steady suction has been used to sort glass particles. This method is found to be preferable to the blowing/suction combination used previously since it minimizes velocity fluctuations. We note two key features of the sorting results: (1) We have been able to sort particles with similar size distributions that differ in density by a factor of four simply by modifying the flow speed appropriately, and (2) For uniform particles, the standard deviations are very low (in most cases, less than 2 μm). Cut sharpness as high as 0.9 were measured.

AVPS is also capable of concentrating air samples. Our measurements indicate that an air sample containing particles with the density of water can be concentrated by a factor of 10.

Future work would include an investigation into the effects of injection location and amount of the particulate on classification accuracy. The addition of a (FPG) Favorable Pressure Gradient could allow for a higher Reynolds number flow while maintaining laminar flow and therefore the accuracy. This would be advantages to applications requiring higher feedrates.

References

[1] Fu, X. K., Gupta, A., McIntyre, P. M., and Phares, D. J., "New Size Sorting Technology for Superconducting Powders," *IEEE Transactions On Appl. Superconductivity*, Vol. 13, 2003, pp. 3494–3497.

[2] Marple, V. A., "History of Impactors - The first 110 years," *Aerosol Science Technology*, Vol. 38, 2004, pp. 247–292.

[3] Torczynski, J. R. and Rader, D. J., "The virtual cyclone: A device fur nonimpact particle separation," *Aerosol Science Technology*, Vol. 26, 1997, pp. 560–573.

[4] Maly, K. and Löffler, F., "Die Strahlumlenkwindsichtung, ein neues Trennverfahren zur wirtschaftlichen Herstellung sehr feinkörniger," *ProduktеActa Pharmaceutica Technologica, APV-Informationsdienst*, Vol. 7, 1979, pp. 27–32.

[5] Romay, F. J., Roberts, D. L., Marple, V. A., Liu, B. Y. H., and Olson, B. A., "A high-performance aerosol concentrator for biological agent detection," *Aerosol Science Technology*, Vol. 36, 2002, pp. 217–226.

[6] Strykowski, P. J., Krothapalli, A., and Forliti, D. J., "Counterflow thrust vectoring," *AIAA J.*, Vol. 34, No. 11, 1996, pp. 2306–2314.

[7] Pack, L. G. and Seifert, A., "Periodic excitation for jet vectoring and enhanced spreading," *J. Aircraft*, Vol. 38, 2001, pp. 486–495.

[8] Pack, L. G. and Seifert, A., "Multiple mode actuation of a turbulent jet," AIAA 39th Aerospace Sciences Meeting, 2001, Paper 2001-0735.

[9] Rapoport, D., Fono, I., Cohen, K., and Seifert, A., "Closed-loop vectoring control of a turbulent jet using periodic excitation," *J. Propulsion Power*, Vol. 19, 2003, pp. 646–654.

[10] Hammond, D. A. and Redekopp, L. G., "Global dynamics and aerodynamic flow vectoring of wakes," *J. Fluid Mech.*, Vol. 338, 1997, pp. 231–248.

[11] Smith, D. R., Parekh, D. E., Kibens, V., and Glezer, A., "Thrust vectoring with hybrid synthetic jet actuators," ASME Fluids Engineering Division Summer Meeting, 1997, Paper FEDSM97-3679.

[12] Smith, B. L. and Glezer, A., "Jet vectoring using synthetic jets," *J. Fluid Mechanics*, Vol. 458, 2002, pp. 1–34.

[13] Guo, D., Cary, A. W., and Agarwal, R. K., "Numerical simulation of vectoring control of a primary jet with a synthetic jet," First AIAA Flow Control Conference, 2002, Paper 2002-3284.

[14] Guo, D., Cary, A. W., and Agarwal, R. K., "Numerical simulation of vectoring of a primary jet with a synthetic jet," *AIAA J.*, Vol. 41, No. 12, 2003, pp. 2364–2370.

[15] Bettridge, M. W., Spall, R. E., and Smith, B. L., "Aerodynamic Jet Steering Using Steady Blowing and Suction," *Exp. Fluids*, Vol. 40, No. 5, 2006, pp. 776–785.

[16] Jackson, D. N. and Smith, B. L., "Theoretical Parameter Study of Aerodynamic Vectoring Particle Sorting," *J. Fluids Eng.*, Vol. 129, 2007, pp. 902–907.

[17] Shapiro, M. and Galperin, V., "Air classification of solid particles: a review," *CHEMICAL ENGINEERING AND PROCESSING*, Vol. 44, No. 2, FEB 2005, pp. 279–285.

[18] Allen, T., *Particle Size Measurement.*, Chapman and Hall Ltd., 1975.

[19] Kim, D., Kim, M., and Lee, K., "Design and performance evaluation of multi-nozzle virtual impactors for concentrating particles," *PARTICLE & PARTICLE SYSTEMS CHARACTERIZATION*, Vol. 17, No. 5-6, DEC 2000, pp. 244–250.

[20] Westerweel, J., "Fundamentals of digital particle image velocimetry," *Measurement Science & Technology*, Vol. 8, 1997, pp. 1379–1392.

[21] Nishino, K., Kato, H., and Torii, K., "Stereo imaging for simultaneous measurement of size and velocity of particles in dispersed two-phase flow," *Meas. Sci. Tech.*, Vol. 11, No. 6, June 2000, pp. 633.

[22] Newman, B. G., "The deflexion of plane jets by adjacent boundaries– Coanda effect," *Boundary Layer and Flow Control*, edited by G. V. Lachmann, Vol. 1, Pergamon Press, 1961.

[23] Neuendorf, R. and Wygnanski, I., "On a turbulent wall jet flowing over a circular cylinder," *J. Fluid Mechanics*, Vol. 381, 1999, pp. 1–25.

Appendix

Chapter A

Drawings of vectoring facility

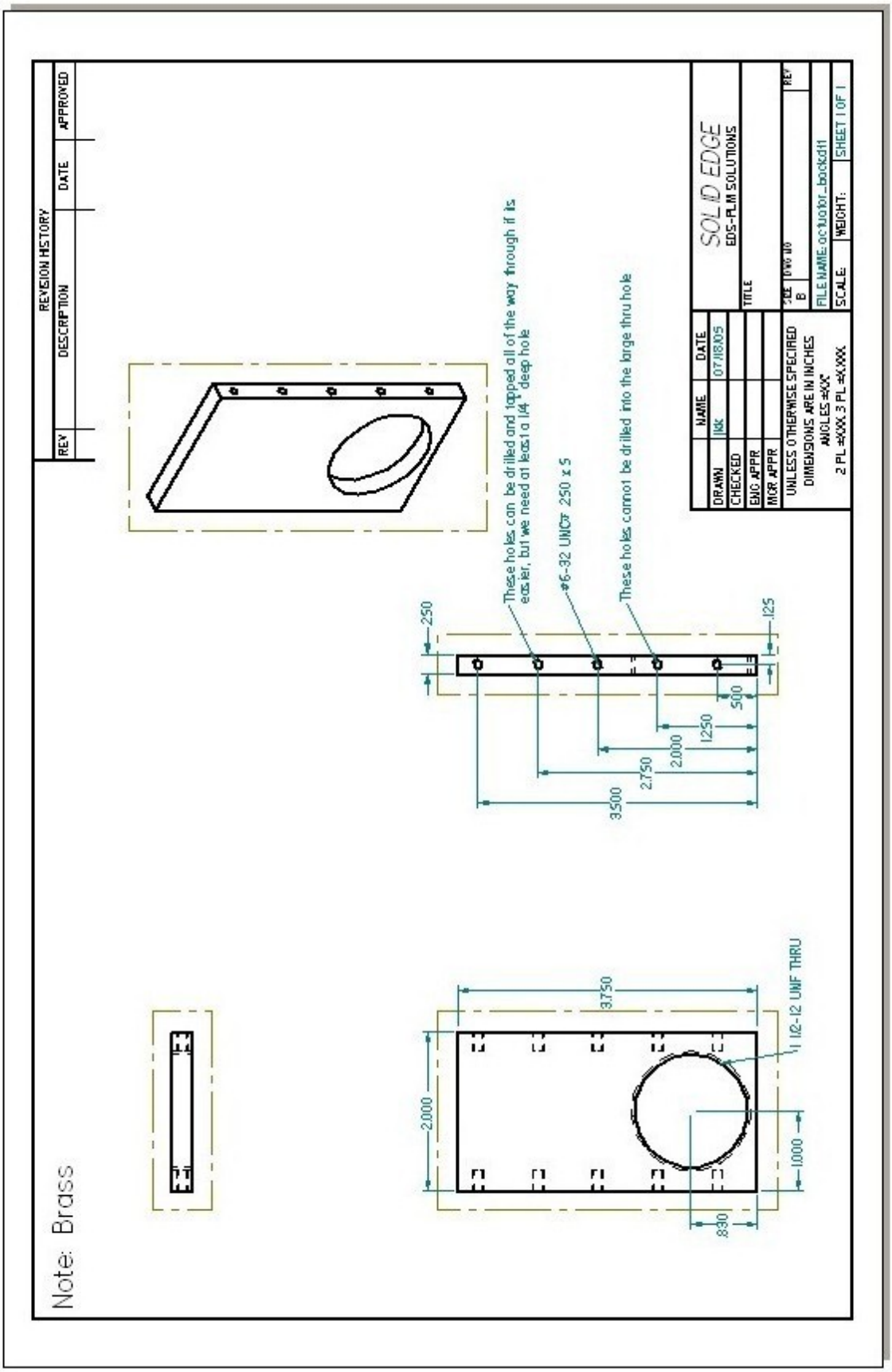
REVISION HISTORY
REV
DESCRIPTION
DATE
APPROVED
Note: Brass
These holes can be drilled and tapped all of the way through if its easier, but we need at least a 1/4" deep hole
#6-32 UNC-B 2B x 5
These holes cannot be drilled into the large thru hole
250
125
500
1250
2000
2750
3500
3750
2000
1000
830
1 1/2-12 UNF THRU
NAME
DATE
DRAWN
WK
07/18/05
CHECKED
ENG APPR.
MGR APPR.
UNLESS OTHERWISE SPECIFIED
DIMENSIONS ARE IN INCHES
ANGLES ±XX°
2 PL ±.XXX 3 PL ±.XXX
SOLID EDGE
EDS-PLM SOLUTIONS
TITLE
SIZE
B
DWG NO
REV
FILE NAME: actuator_backdll
SCALE:
WEIGHT:
SHEET 1 OF 1

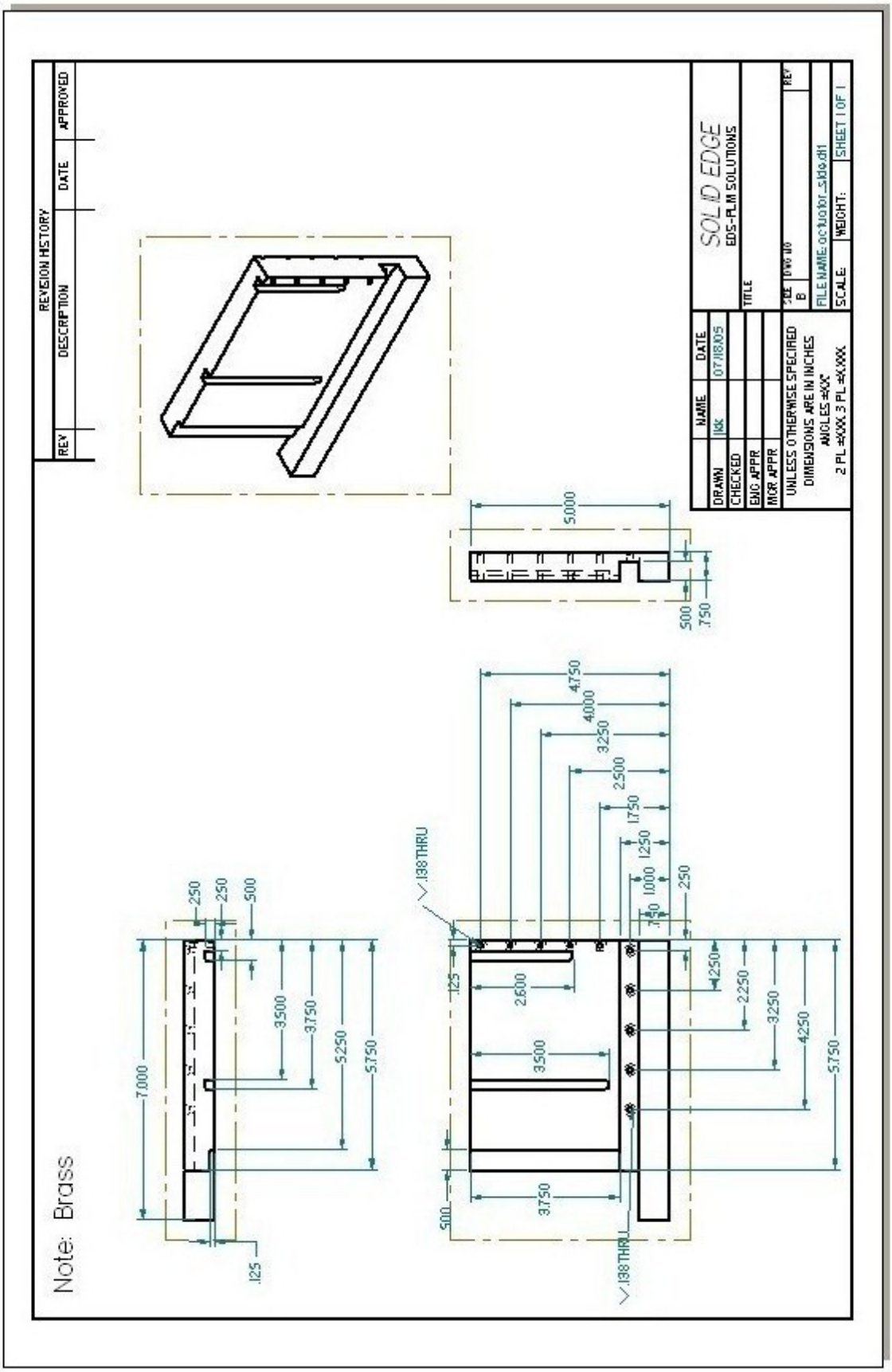
REVISION HISTORY
REV
DESCRIPTION
DATE
APPROVED
Note: Brass
SOLID EDGE
EDS-PLM SOLUTIONS
NAME
DATE
DRAWN
CHECKED
ENG APPR.
MGR APPR.
UNLESS OTHERWISE SPECIFIED
DIMENSIONS ARE IN INCHES
ANGLES ±XX°
2 PL ±XXX, 3 PL ±X.XXX
TITLE
SIZE
B
DWG NO
REV
FILE NAME
SCALE:
WEIGHT:
SHEET 1 OF 1
.138 THRU
.138 THRU
5.000
.500
.750
.250
.250
.500
7.000
3.500
3.750
5.250
5.750
.125
.125
.500
2.600
3.500
3.750
4.750
4.000
3.250
2.500
1.750
1.250
1.000
.750
.250
.250
2.250
3.250
4.250
5.750

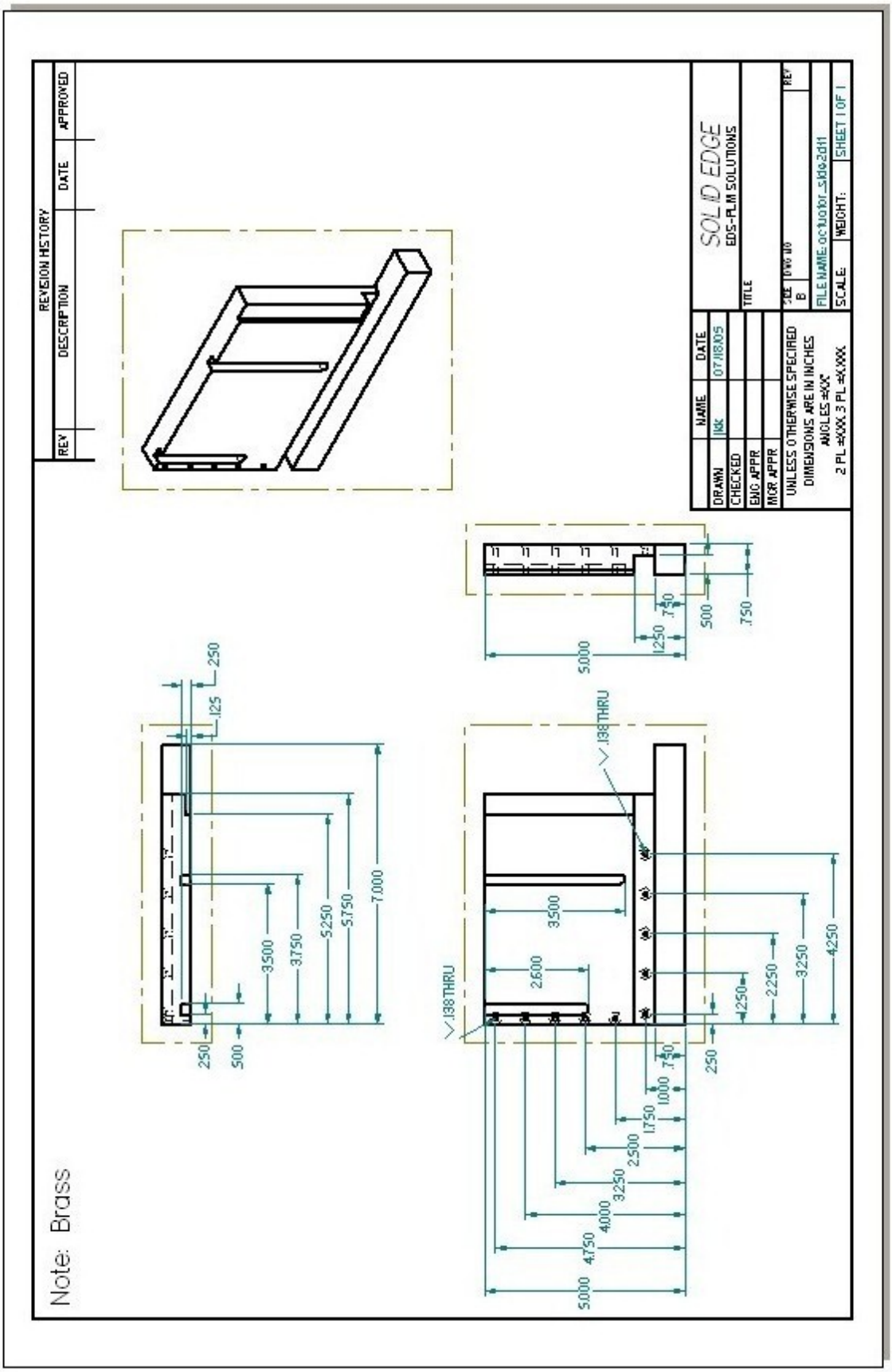
REVISION HISTORY
REV
DESCRIPTION
DATE
APPROVED
Note: Brass
SOLID EDGE
EDS-PLM SOLUTIONS
NAME
DATE
DRAWN
CHECKED
ENG APPR.
MGR APPR.
UNLESS OTHERWISE SPECIFIED
DIMENSIONS ARE IN INCHES
ANGLES ±XX°
2 PL ±XXX 3 PL ±XXXX
TITLE
SIZE
B
DWG NO
REV
FILE NAME
SCALE:
WEIGHT:
SHEET 1 OF 1
.138 THRU
.138 THRU
.250
.125
.500
3.500
3.750
5.250
5.750
7.000
.250
.500
.750
1.250
5.000
.750
1.000
1.750
2.500
3.250
4.000
4.750
5.000
.250
2.600
3.500
.250
2.250
3.250
4.250

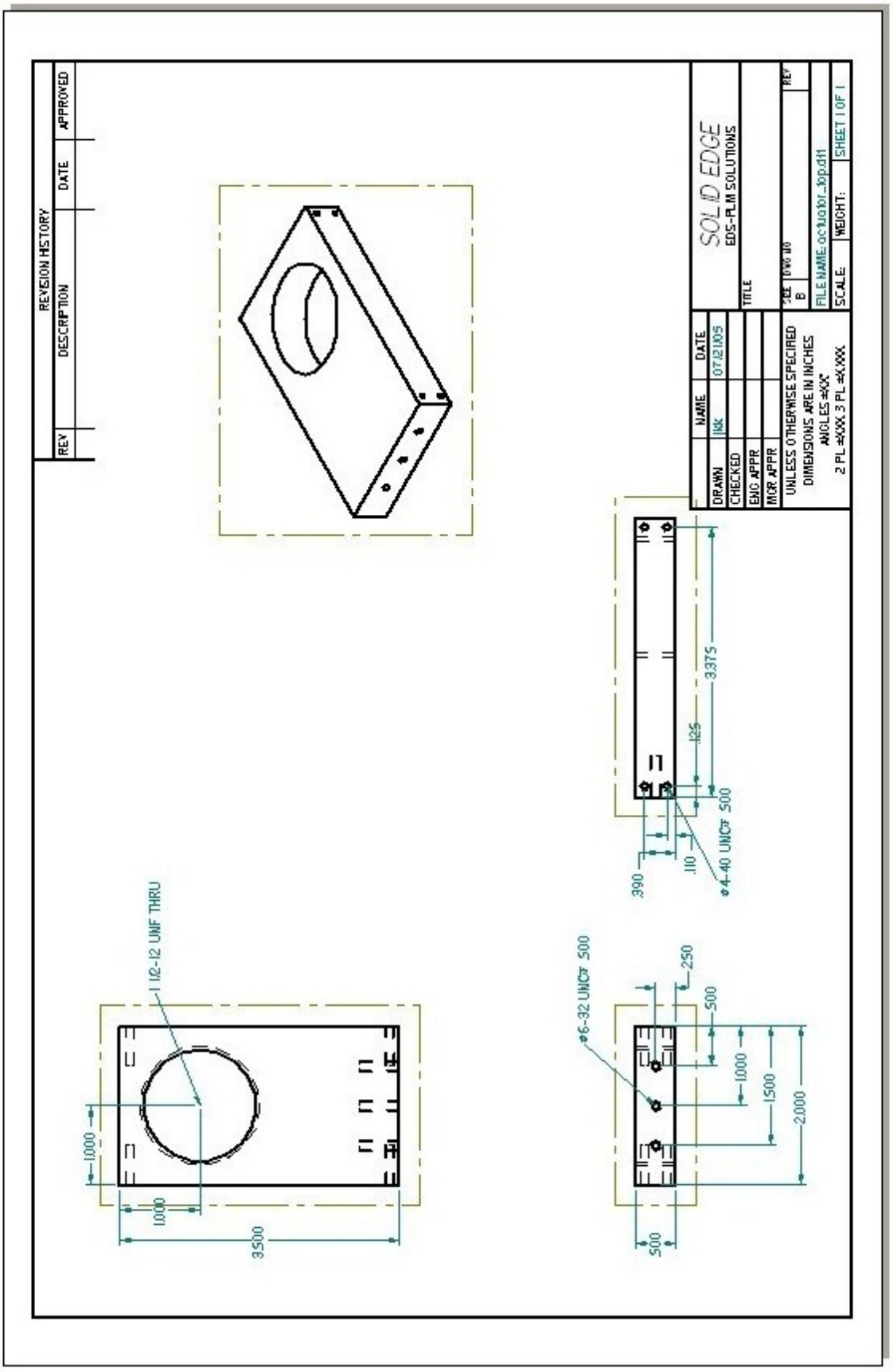
REVISION HISTORY
REV
DESCRIPTION
DATE
APPROVED
SOLID EDGE
EDS-PLM SOLUTIONS
NAME
DATE
DRAWN
WK
07/21/05
CHECKED
ENG APPR
MGR APPR
TITLE
SIZE
B
DWG NO
REV
UNLESS OTHERWISE SPECIFIED
DIMENSIONS ARE IN INCHES
ANGLES ±XX°
2 PL ±XXX 3 PL ±XXXX
FILE NAME: actuator_top.dft
SCALE:
WEIGHT:
SHEET 1 OF 1
1.000
1.000
3.500
1/2-12 UNF THRU
.500
1.000
1.500
2.000
.250
#6-32 UNC-2B .500
.500
.390
.110
#4-40 UNC-2B .500
.125
3.375

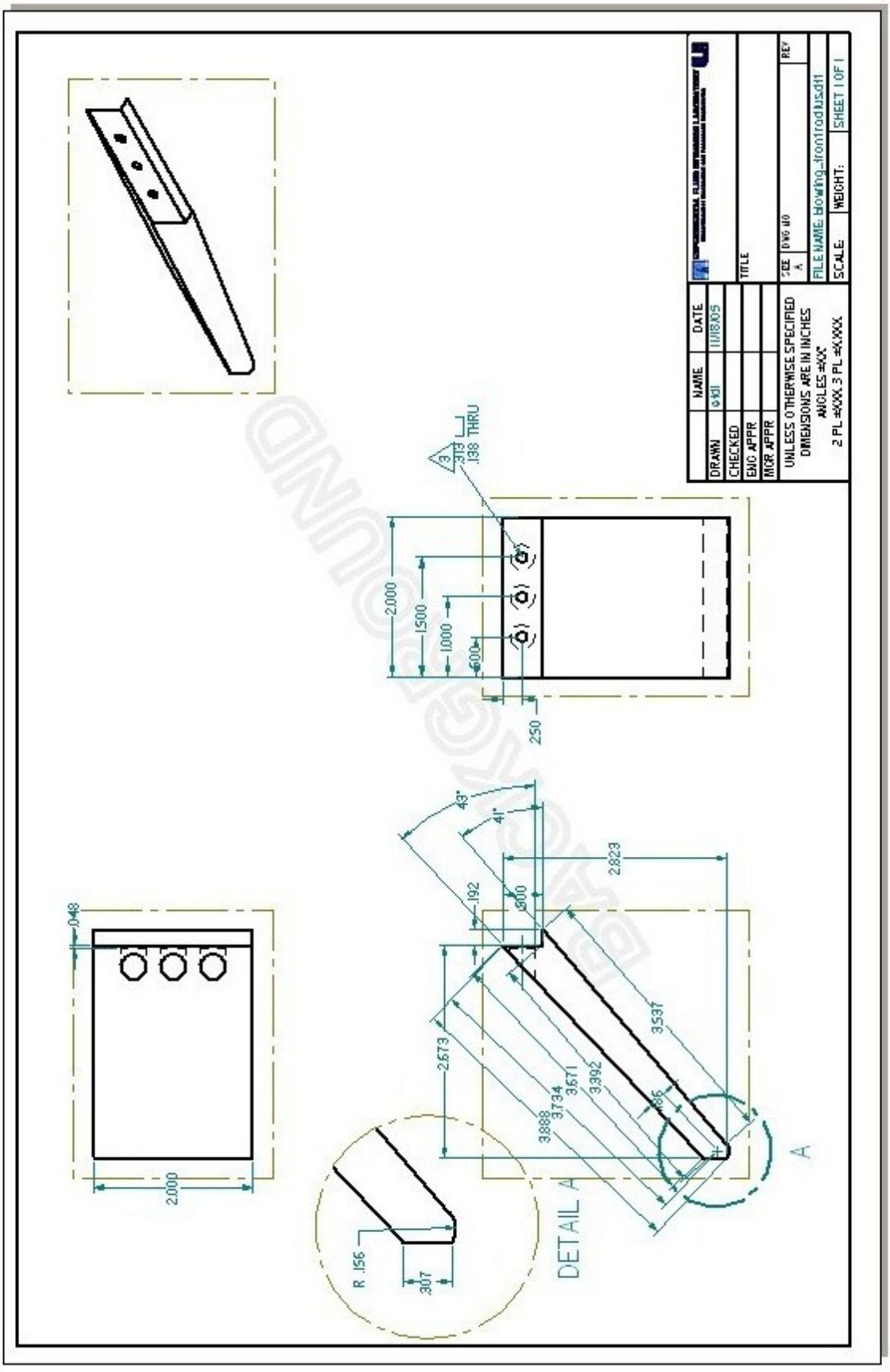
NAME
DATE
DRAWN
CHECKED
ENG APPR
MGR APPR
UNLESS OTHERWISE SPECIFIED
DIMENSIONS ARE IN INCHES
ANGLES ±0.5°
2 PL ±.XXX 3 PL ±.XXXX
TITLE
SIZE
A
DWG NO
REV
FILE NAME: Browning_frontrodMsdt1
SCALE:
WEIGHT:
SHEET 1 OF 1
.048
2.000
.9
.375
.138 THRU
2.000
1.500
1.000
.600
250
43°
41°
.192
.600
2.823
2.673
3.537
3.888
3.734
3.671
3.392
.186
DETAIL A
R .156
.307
A

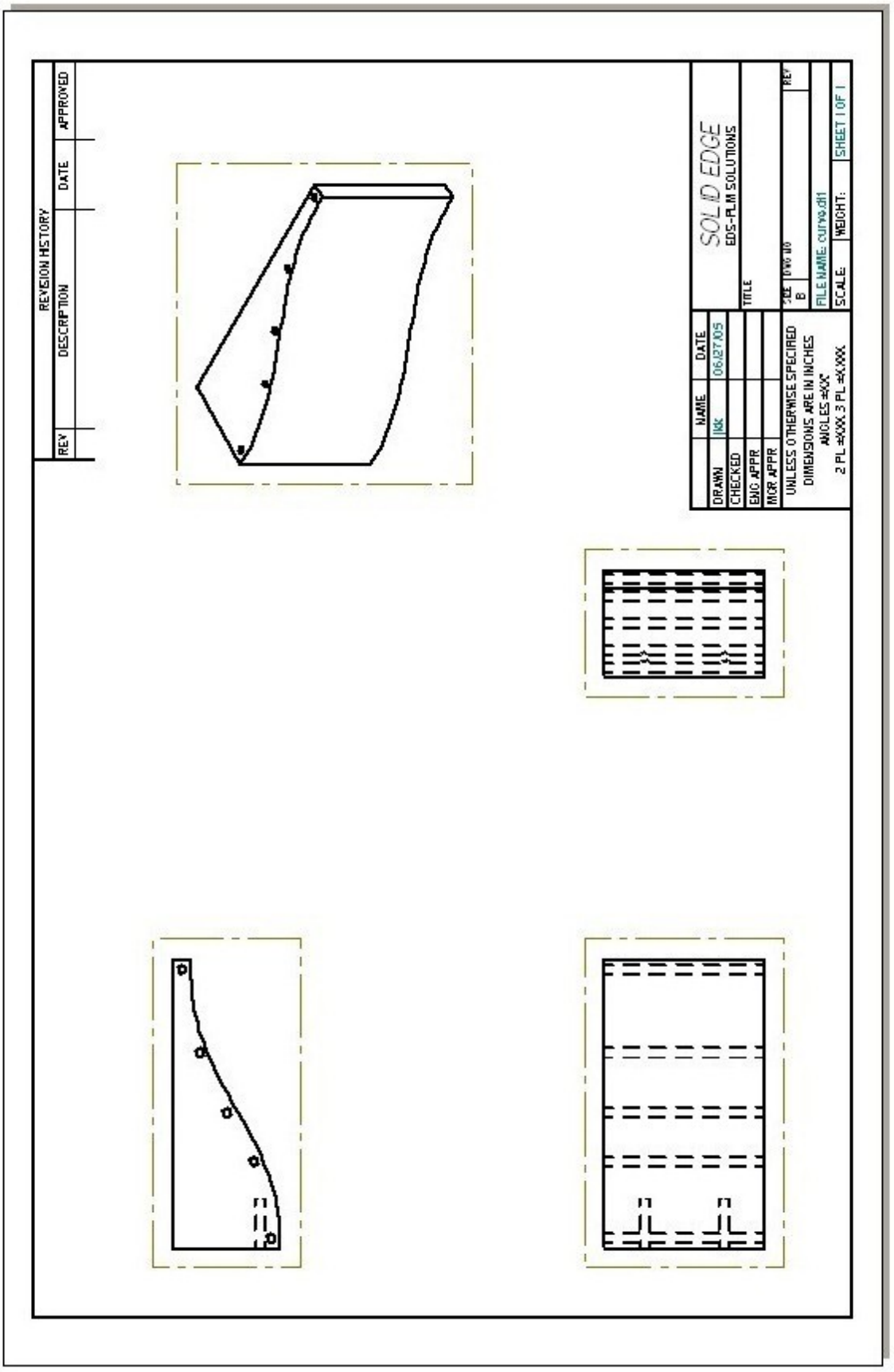
REVISION HISTORY
REV
DESCRIPTION
DATE
APPROVED
SOLID EDGE
EDS-PLM SOLUTIONS
NAME
DATE
DRAWN
06/27/05
CHECKED
ENG APPR.
MGR APPR.
TITLE
SIZE
B
DWG NO
REV
UNLESS OTHERWISE SPECIFIED
DIMENSIONS ARE IN INCHES
ANGLES ±XX°
2 PL ±XXX 3 PL ±X.XXX
FILE NAME: curve.dft
SCALE:
WEIGHT:
SHEET 1 OF 1

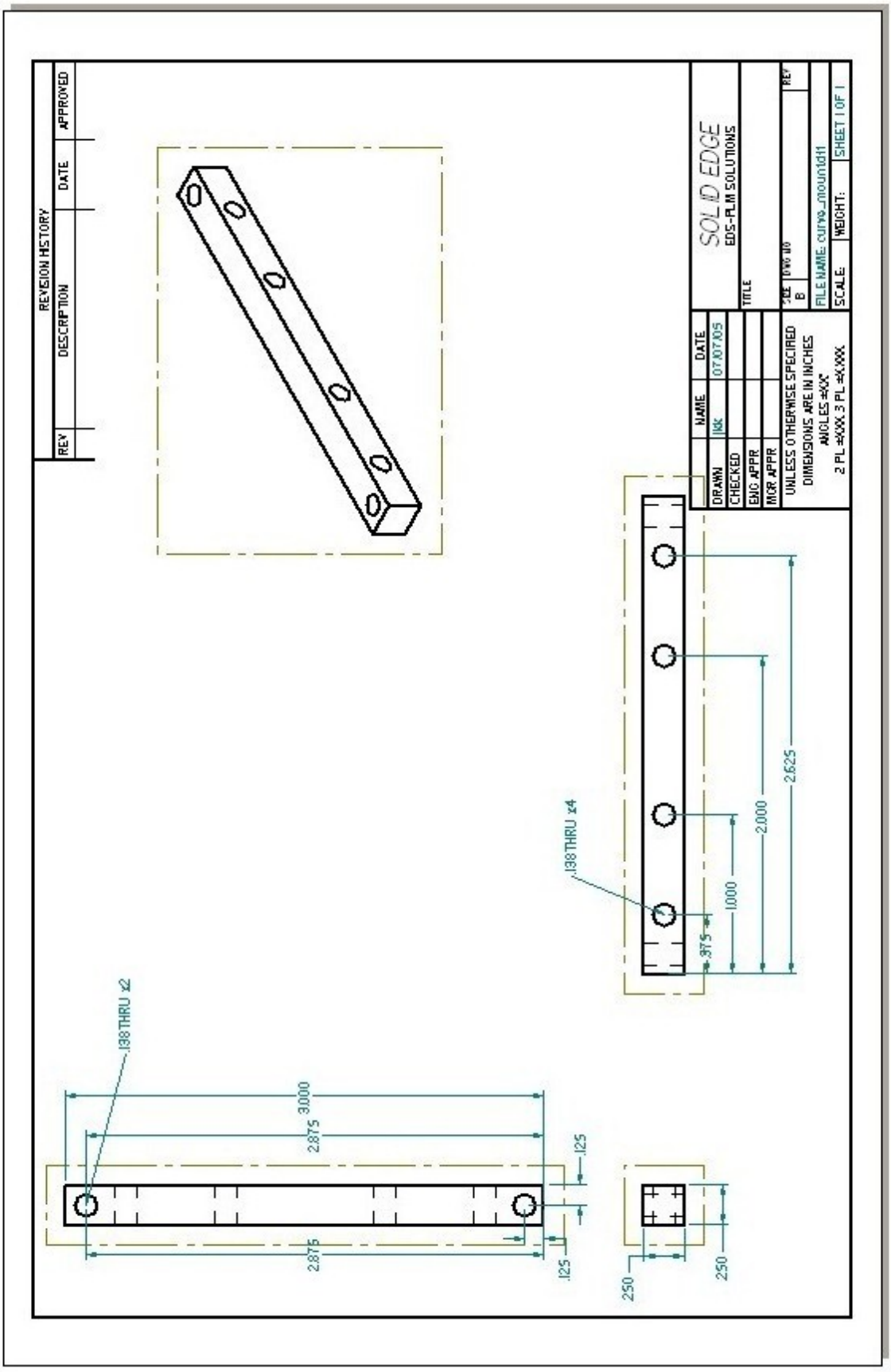
REVISION HISTORY
REV
DESCRIPTION
DATE
APPROVED
SOLID EDGE
EDS-PLM SOLUTIONS
NAME
DATE
DRAWN
MK
07.07.05
CHECKED
ENG APPR.
MGR APPR.
TITLE
SIZE
B
DWG NO
REV
UNLESS OTHERWISE SPECIFIED
DIMENSIONS ARE IN INCHES
ANGLES ±XX°
2 PL ±XXX, 3 PL ±X.XXX
FILE NAME: curve_mount1d11
SCALE:
WEIGHT:
SHEET 1 OF 1
.138 THRU x4
.375
1.000
2.000
2.625
.138 THRU x2
3.000
2.875
.125
.250

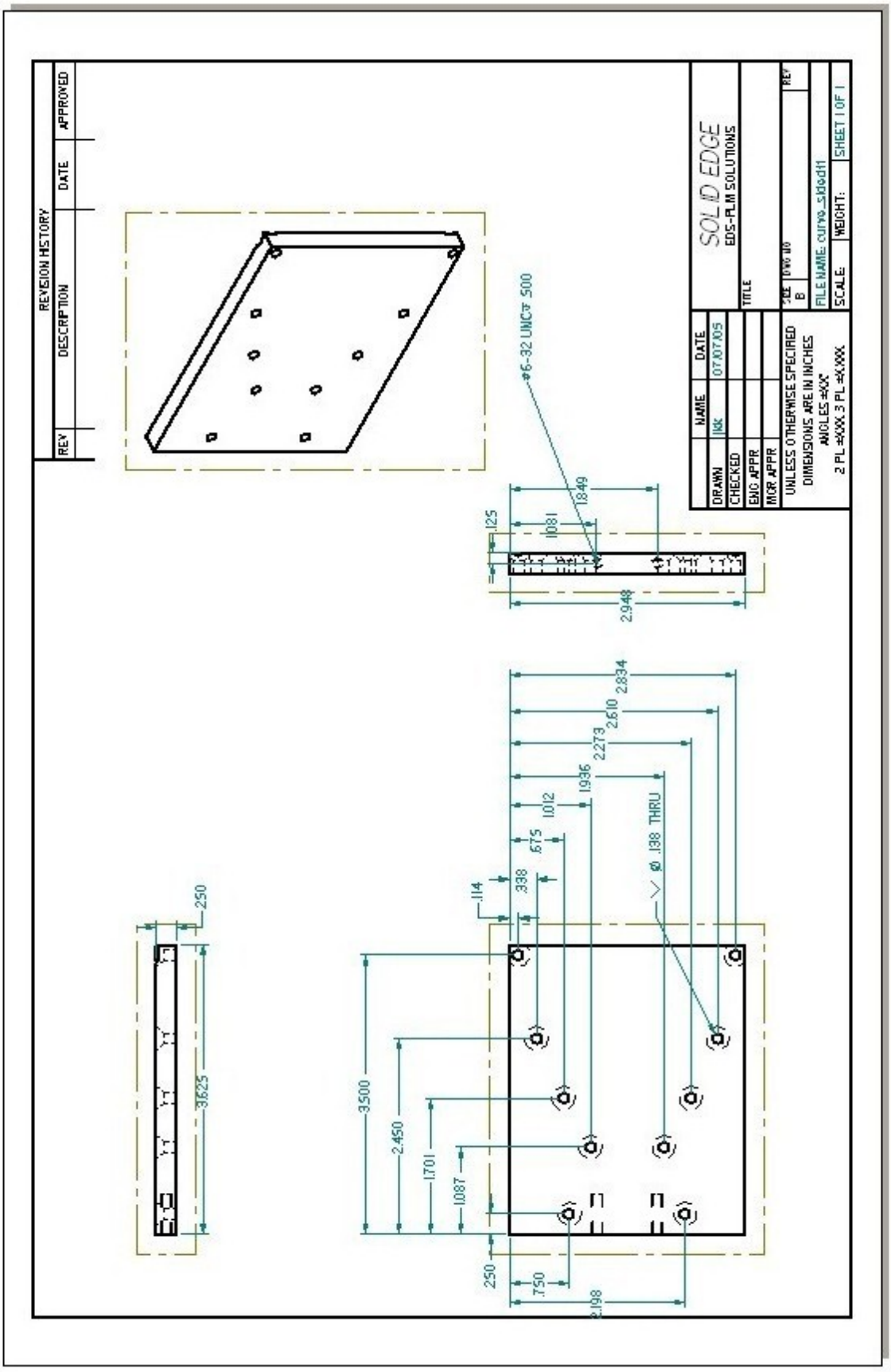
REVISION HISTORY
REV
DESCRIPTION
DATE
APPROVED
SOLID EDGE
EDS-PLM SOLUTIONS
NAME
DATE
DRAWN
MK
07.07.05
CHECKED
ENG APPR.
MGR APPR.
TITLE
UNLESS OTHERWISE SPECIFIED
DIMENSIONS ARE IN INCHES
ANGLES ±XX°
2 PL ±.XXX 3 PL ±.XXX
SIZE
B
DWG NO
REV
FILE NAME: curve_sklodi1
SCALE:
WEIGHT:
SHEET 1 OF 1
#6-32 UNC-2 500
.125
1.081
1.849
2.948
.250
3.625
.114
.338
.675
1.012
1.936
2.273
2.610
2.834
Ø .138 THRU
3.500
2.450
1.701
1.087
.250
.750
2.198

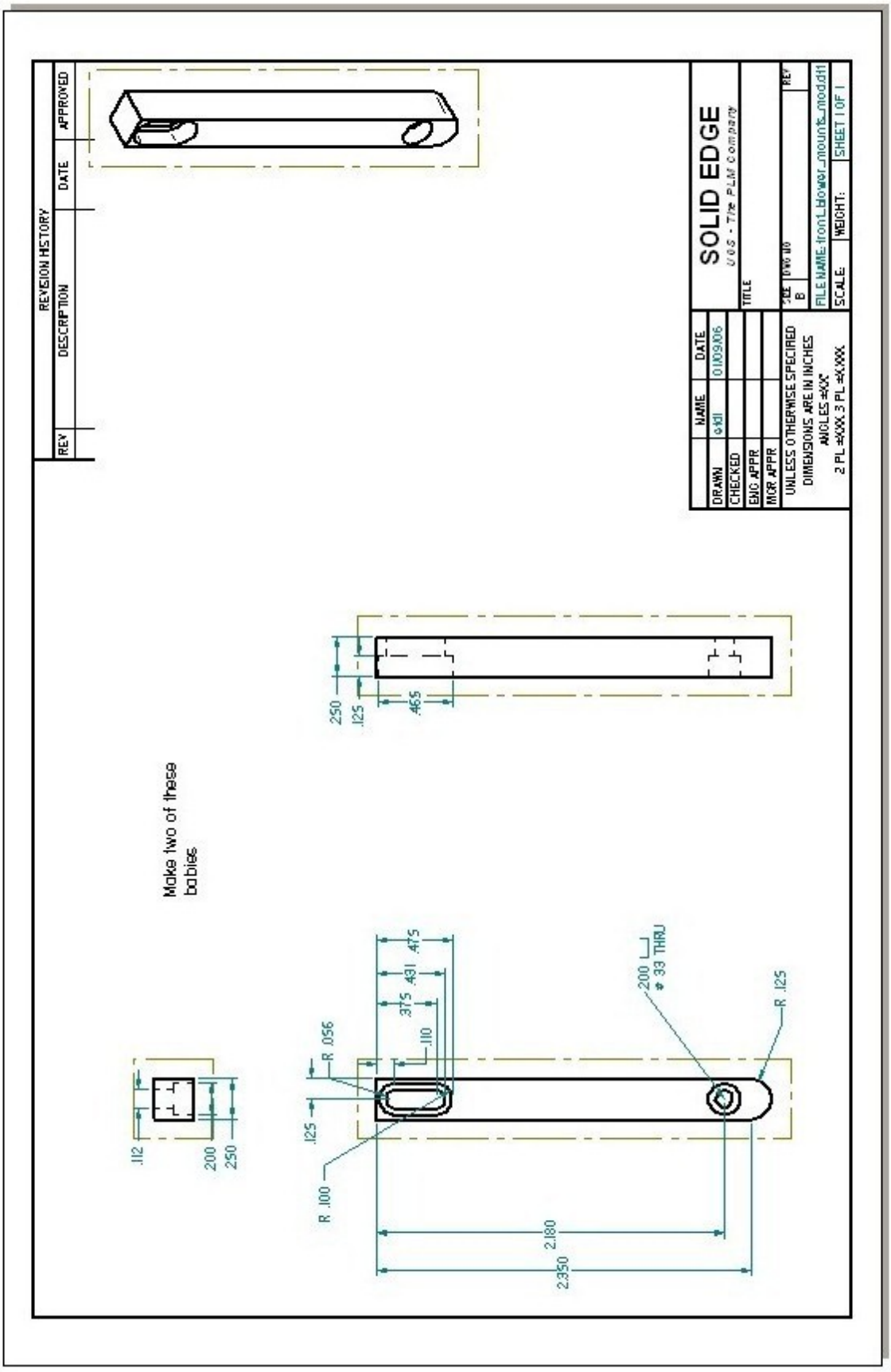
REVISION HISTORY
REV
DESCRIPTION
DATE
APPROVED
SOLID EDGE
UGS - The PLM Company
NAME
DATE
DRAWN
CHECKED
ENG APPR.
MGR APPR.
TITLE
UNLESS OTHERWISE SPECIFIED
DIMENSIONS ARE IN INCHES
ANGLES ±XX°
2 PL ±XXX, 3 PL ±XXXX
SIZE
B
DWG NO
REV
FILE NAME: frontL_blower_mount_mod.dft
SCALE:
WEIGHT:
SHEET 1 OF 1
Make two of these babies
.112
.200
.250
.125
R .100
R .056
.375
.431
.475
.110
.200
33 THRU
R .125
2.180
2.350
.250
.125
.465

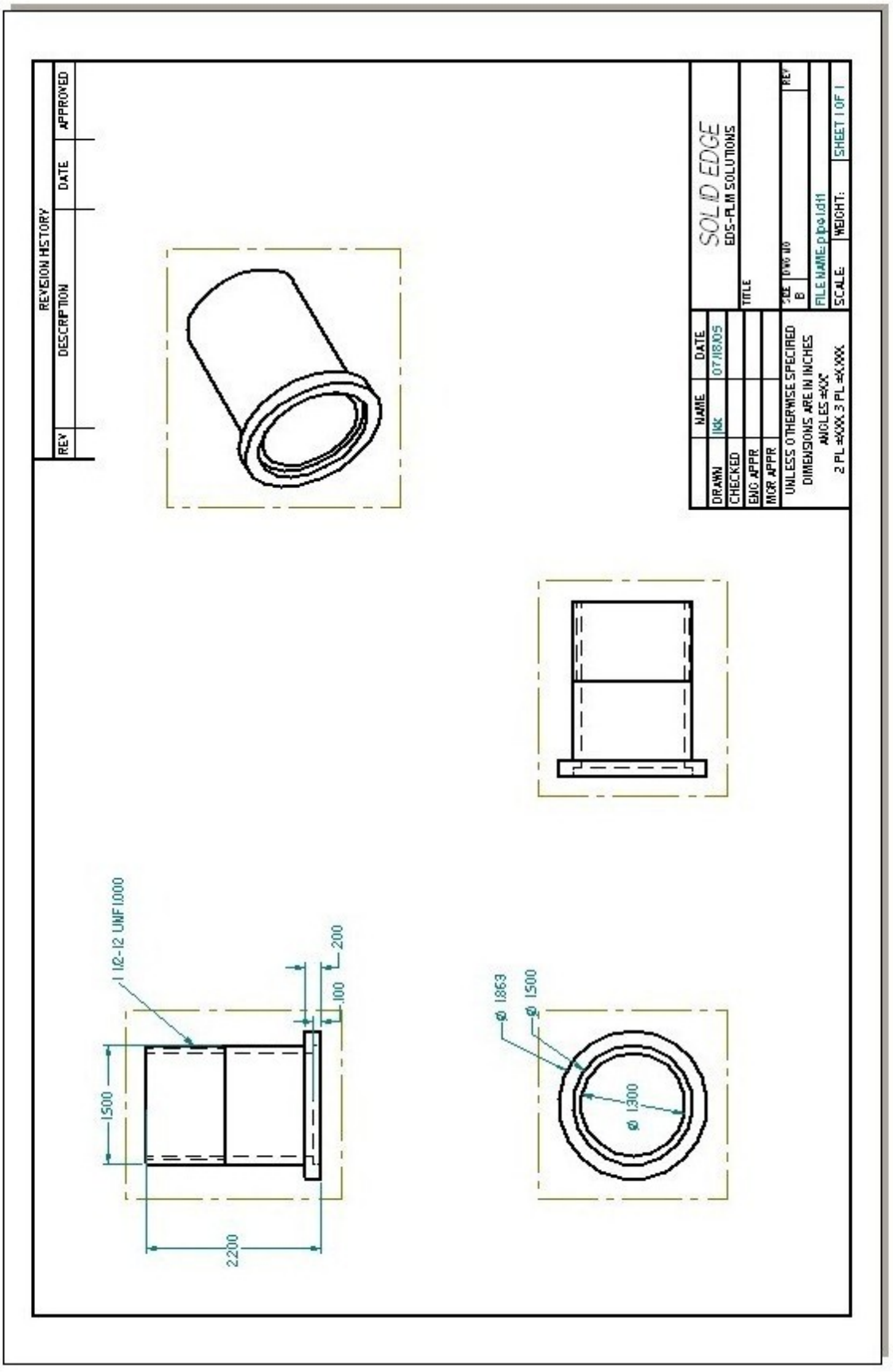
REVISION HISTORY
REV
DESCRIPTION
DATE
APPROVED
SOLID EDGE
EDS-PLM SOLUTIONS
NAME
DATE
DRAWN
CHECKED
ENG APPR.
MGR APPR.
TITLE
UNLESS OTHERWISE SPECIFIED
DIMENSIONS ARE IN INCHES
ANGLES ±XX°
2 PL ±.XXX 3 PL ±.XXX
SIZE
B
DWG NO
REV
FILE NAME: pipe1.dft
SCALE:
WEIGHT:
SHEET 1 OF 1
1 1/2-12 UNF 1.000
.200
.100
1.500
2.200
Ø .1863
Ø 1.500
Ø 1.300

REVISION HISTORY			
REV	DESCRIPTION	DATE	APPROVED

Note: The tabs on the pipe are not to be included

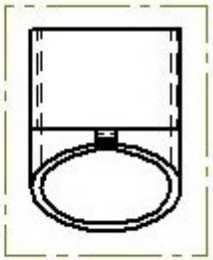

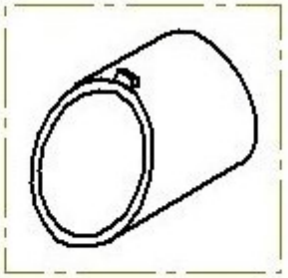

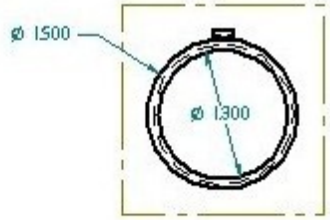

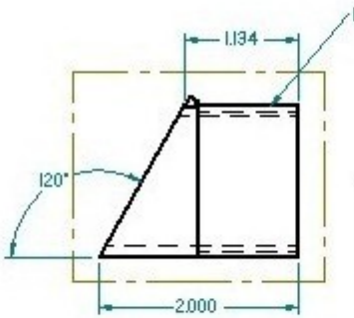

	NAME	DATE
DRAWN	kk	07/29/05
CHECKED		
ENG APPR		
MGR APPR		

UNLESS OTHERWISE SPECIFIED
DIMENSIONS ARE IN INCHES
ANGLES ±XX°
2 PL ±XXX 3 PL ±XXXX

SOLID EDGE
EDS-PLM SOLUTIONS

TITLE

SIZE B | DWG NO | REV

FILE NAME: pipe2d11

SCALE: | WEIGHT: | SHEET 1 OF 1

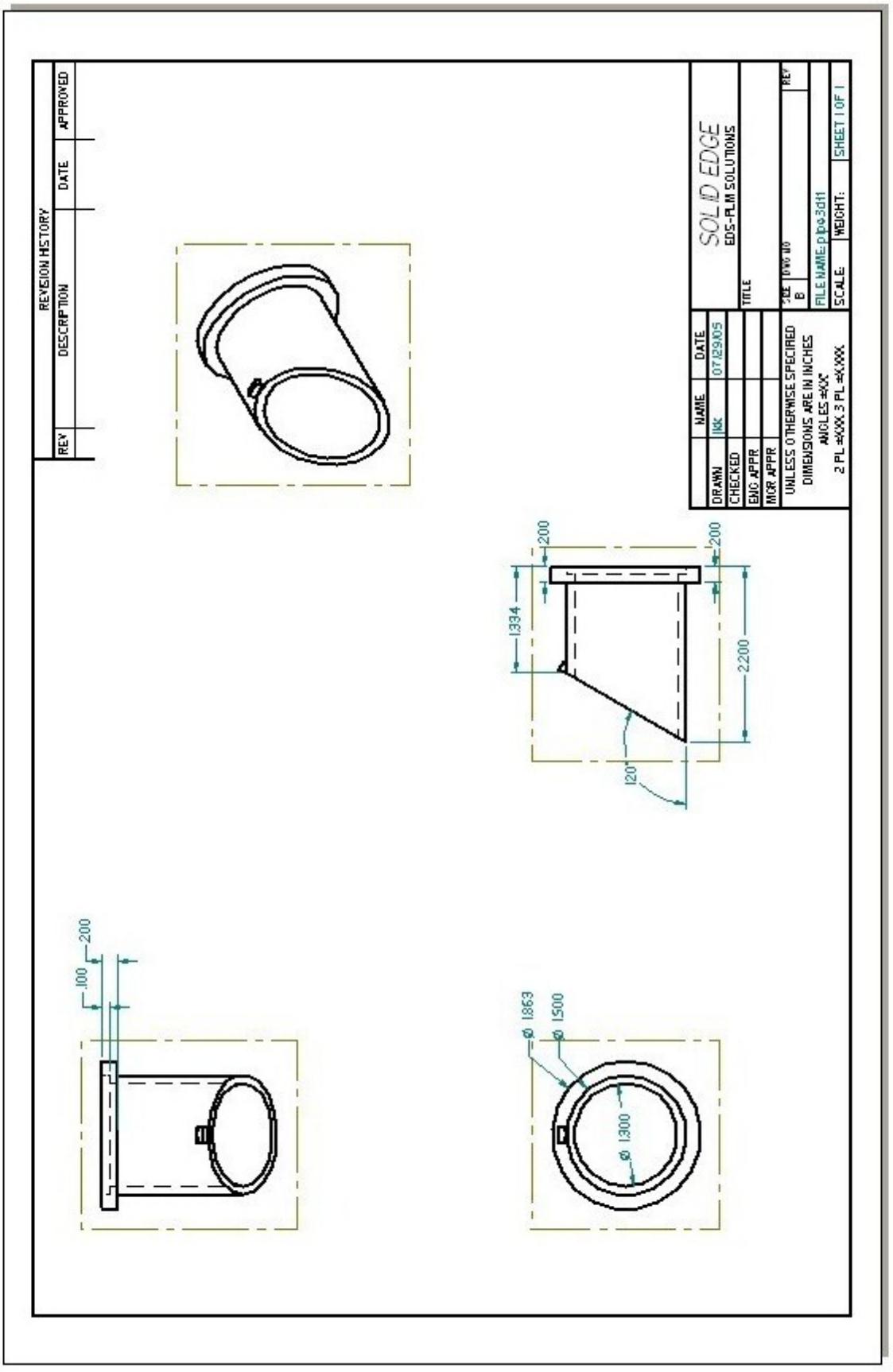
REVISION HISTORY
REV
DESCRIPTION
DATE
APPROVED
SOLID EDGE
EDS-PLM SOLUTIONS
NAME
DATE
DRAWN
MK
07/29/05
CHECKED
ENG APPR.
MGR APPR.
TITLE
SIZE
B
DWG NO
REV
UNLESS OTHERWISE SPECIFIED
DIMENSIONS ARE IN INCHES
ANGLES ±XX°
2 PL ±XXX, 3 PL ±X.XXX
FILE NAME: pipe3dfl
SCALE:
WEIGHT:
SHEET 1 OF 1
.200
.100
1.334
2.200
120°
Ø 1.863
Ø 1.500
Ø 1.300

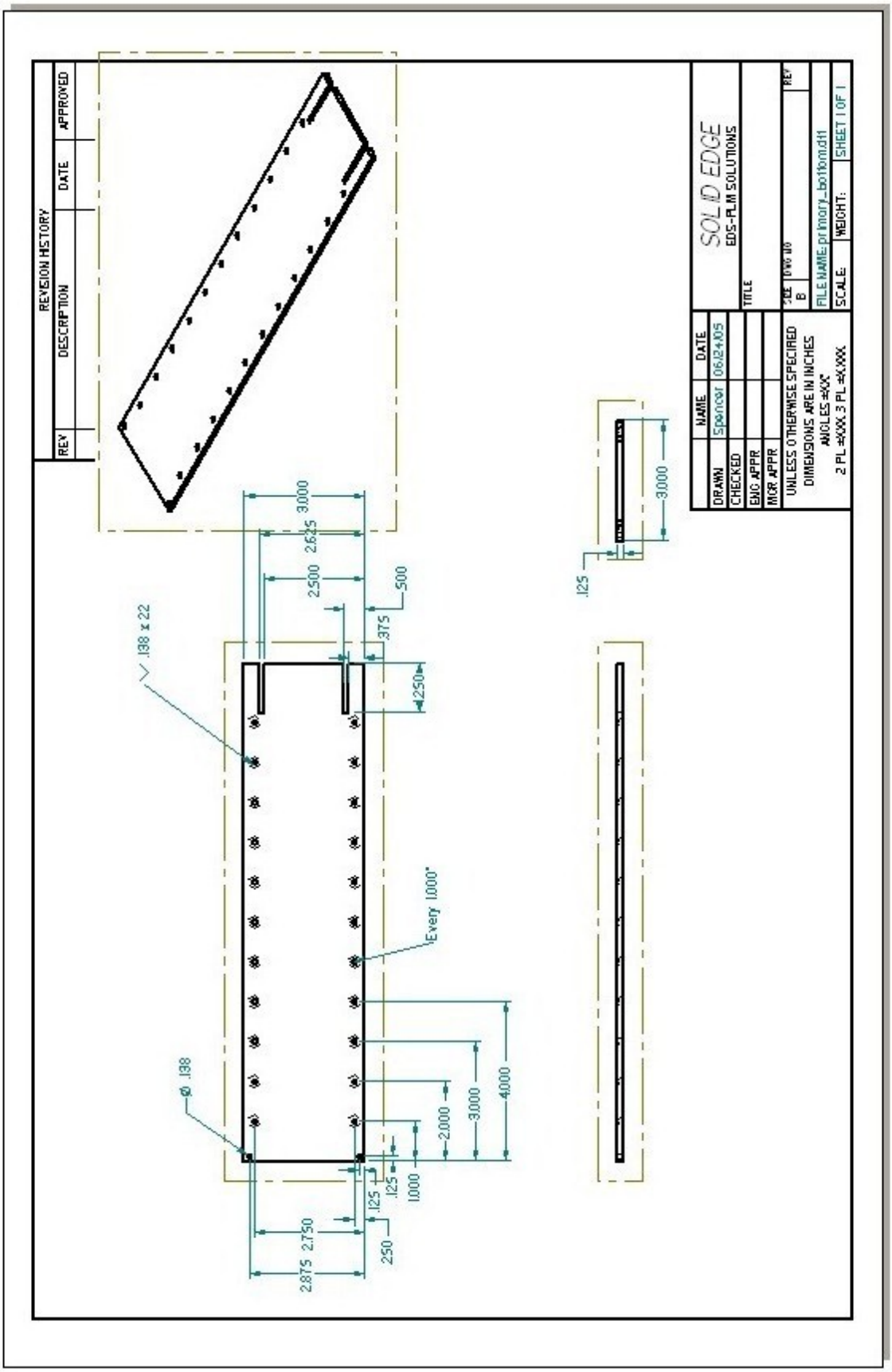
REVISION HISTORY
REV
DESCRIPTION
DATE
APPROVED
NAME
DATE
DRAWN
Spencer
06/24/05
CHECKED
ENG APPR.
MGR APPR.
SOLID EDGE
EDS-PLM SOLUTIONS
TITLE
SIZE
B
DWG NO
REV
UNLESS OTHERWISE SPECIFIED
DIMENSIONS ARE IN INCHES
ANGLES ±XX°
2 PL ±XXX 3 PL ±X.XXX
FILE NAME: primary_bottom.dft
SCALE:
WEIGHT:
SHEET 1 OF 1
.138 x 22
Ø .138
Every 1.000"
.125
3.000
2.625
2.500
.500
.375
.250
2.750
2.875
1.000
2.000
4.000

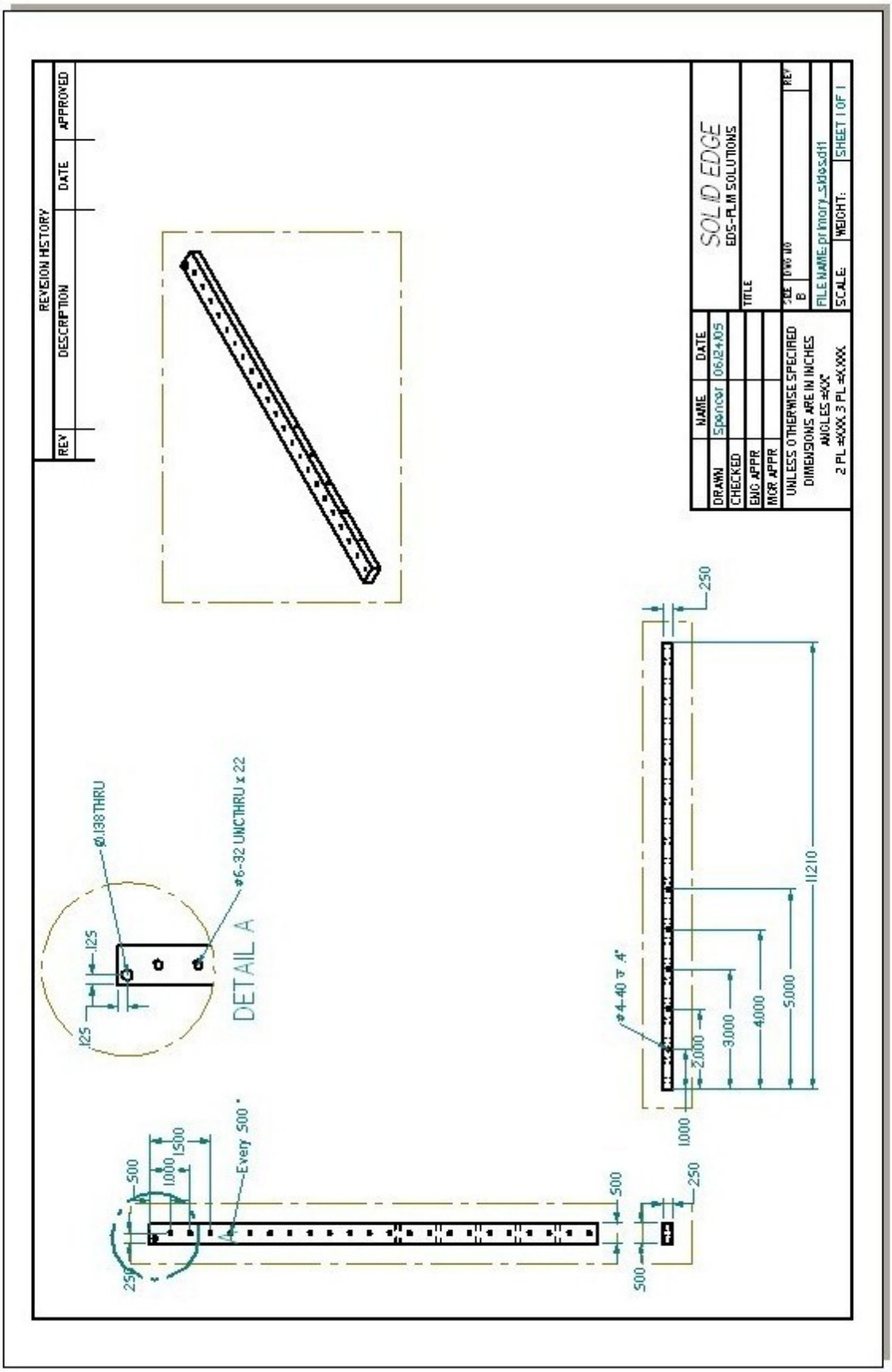
REVISION HISTORY
REV
DESCRIPTION
DATE
APPROVED
SOLID EDGE
EDS-PLM SOLUTIONS
NAME
DATE
DRAWN
Spencer
06/24/05
CHECKED
ENG APPR.
MGR APPR.
TITLE
UNLESS OTHERWISE SPECIFIED
DIMENSIONS ARE IN INCHES
ANGLES ±XX°
2 PL ±XXX 3 PL ±X.XXX
SIZE
B
DWG NO
REV
FILE NAME: primary_s.dwsdft
SCALE:
WEIGHT:
SHEET 1 OF 1
DETAIL A
Ø.138 THRU
#6-32 UNC THRU x 22
.125
.125
#4-40 x .4"
Every 500
500
1000
1500
250
500
250
1000
2000
3000
4000
5000
11210
250
500

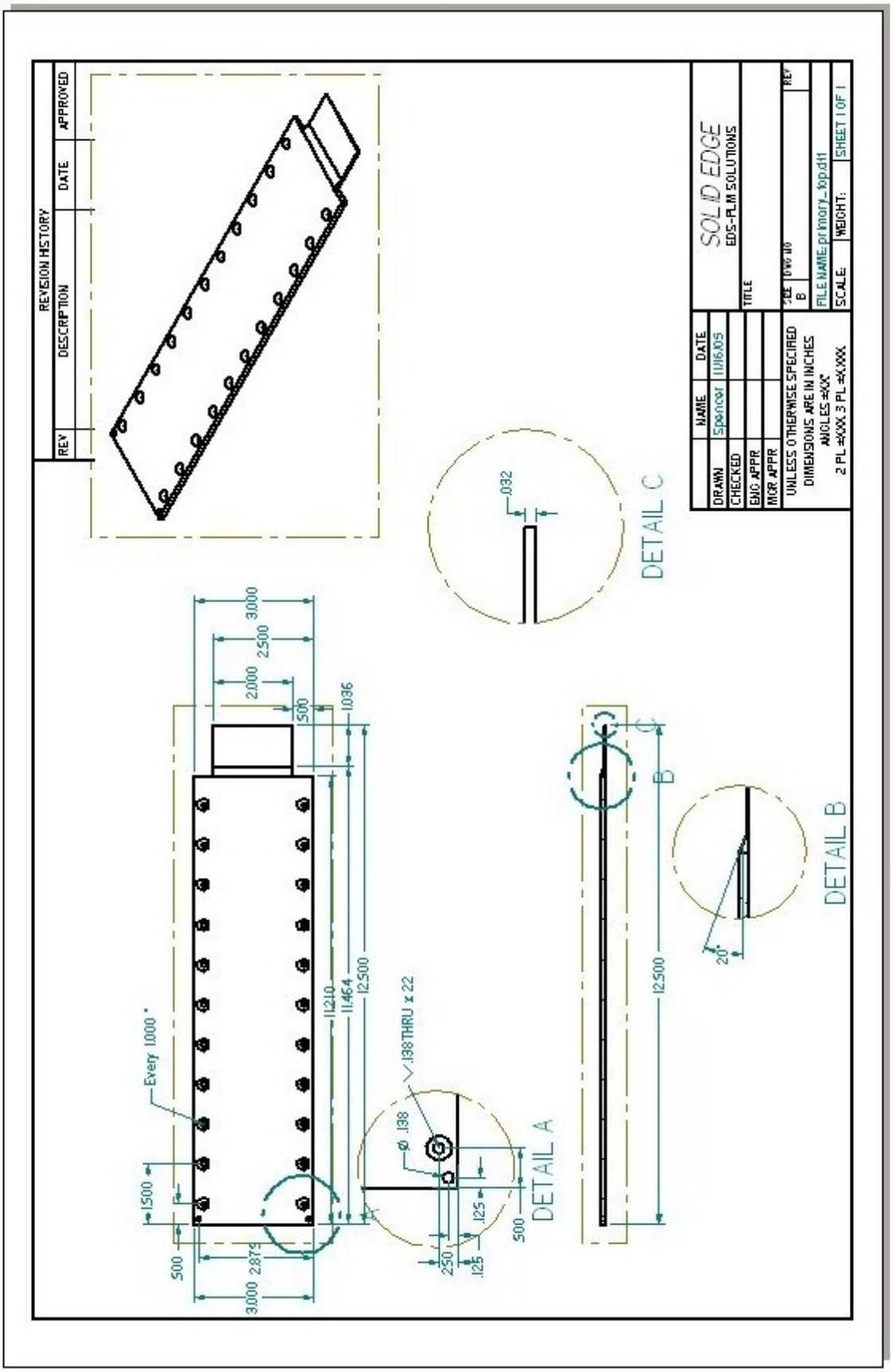
REVISION HISTORY
REV
DESCRIPTION
DATE
APPROVED
DETAIL A
DETAIL B
DETAIL C
Every 1.000 "
.138 THRU x 22
Ø .138
.032
20°
SOLID EDGE
EDS-PLM SOLUTIONS
DRAWN
Spencer
11/16/05
CHECKED
ENG APPR.
MGR APPR.
TITLE
UNLESS OTHERWISE SPECIFIED
DIMENSIONS ARE IN INCHES
ANGLES ±XX°
2 PL ±.XXX, 3 PL ±.XXX
SIZE
B
DWG NO
REV
FILE NAME: primary_top.dft
SCALE:
WEIGHT:
SHEET 1 OF 1

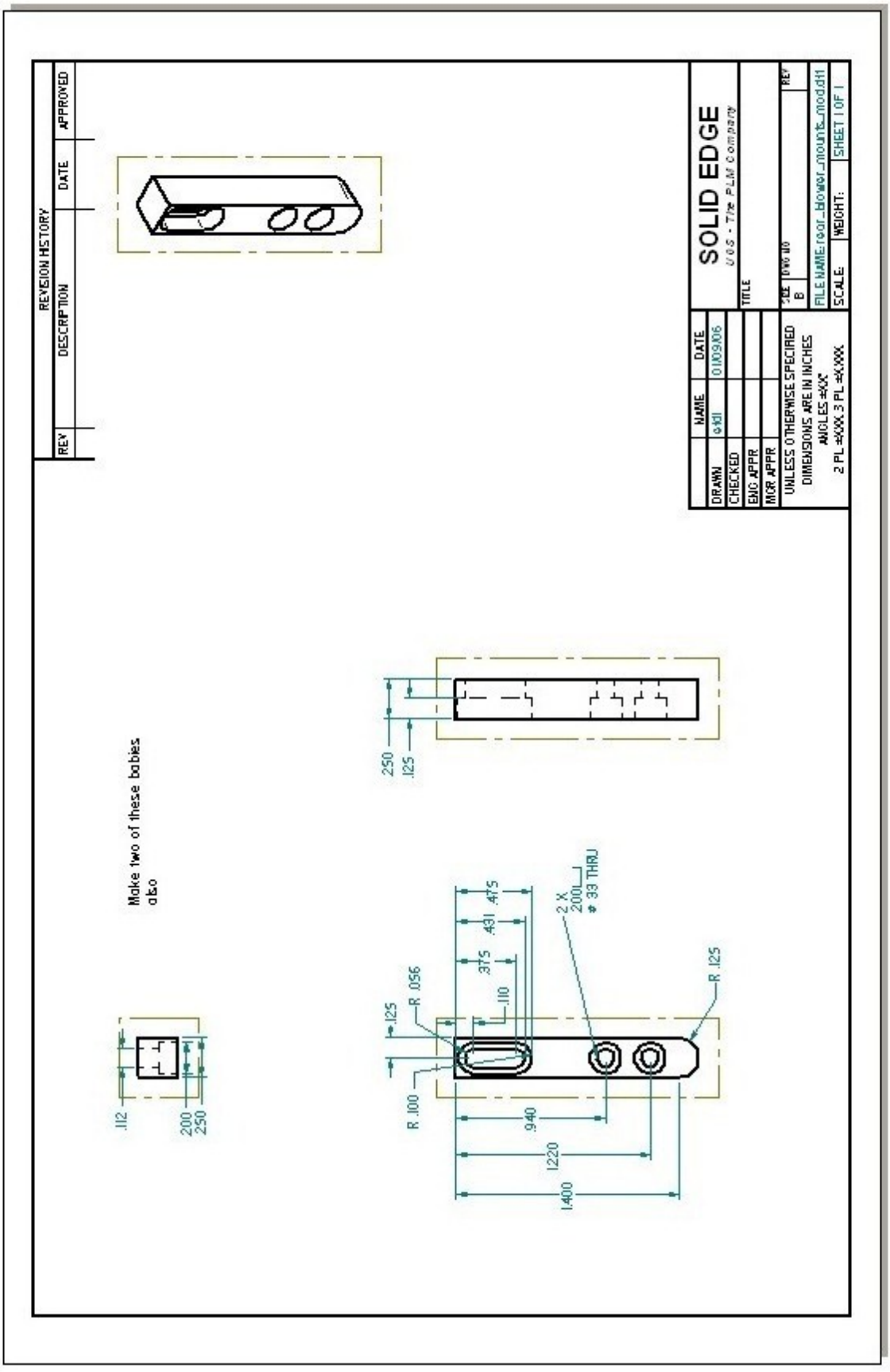
REVISION HISTORY
REV
DESCRIPTION
DATE
APPROVED
SOLID EDGE
V16 - The PLM Company
NAME
DATE
DRAWN
CHECKED
ENG APPR.
MGR APPR.
TITLE
SIZE
B
DWG NO
REV
UNLESS OTHERWISE SPECIFIED
DIMENSIONS ARE IN INCHES
ANGLES ±XX°
2 PL ±XXX 3 PL ±XXXX
FILE NAME: rear_blower_mounts_mod.dft
SCALE:
WEIGHT:
SHEET 1 OF 1
Make two of these babies
also
.112
200
250
250
.125
.125
R .056
R .100
.375
.431
.475
.110
2 X
.200
Ø .33 THRU
R .125
.940
1.220
1.400

NOTE: The radiused edge is on the bottom only.

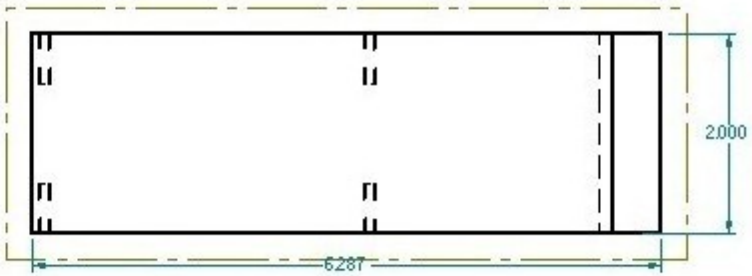

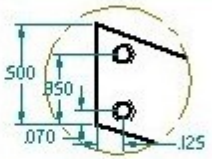

DETAIL A

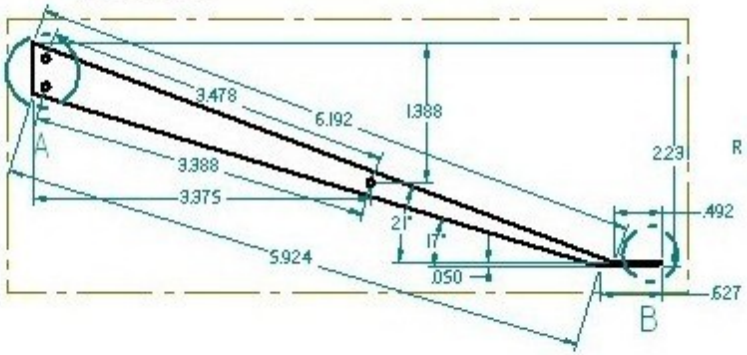

DETAIL B

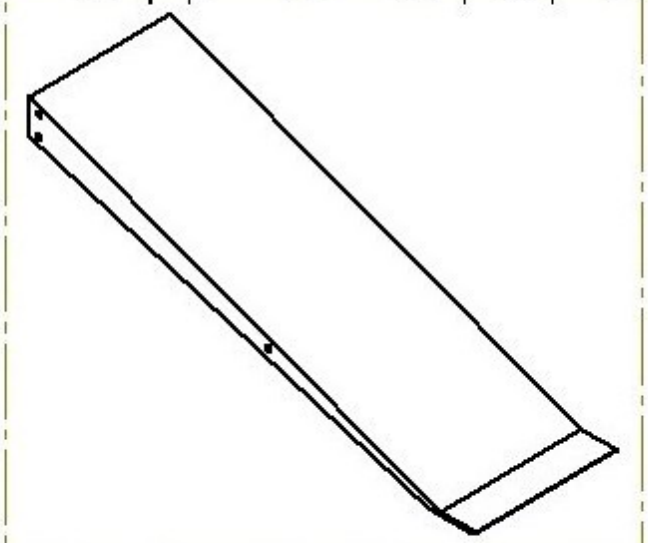

REVISION HISTORY			
REV	DESCRIPTION	DATE	APPROVED

	NAME	DATE
DRAWN	eldl	11/07/05
CHECKED		
ENG APPR		
MGR APPR		

UNLESS OTHERWISE SPECIFIED
DIMENSIONS ARE IN INCHES
ANGLES ±XX°
2 PL ±XXX 3 PL ±XXXX

SOLID EDGE
EDS-PLM SOLUTIONS

TITLE

SIZE B | DWG NO | REV

FILE NAME: suction mod file.dft1

SCALE: | WEIGHT: | SHEET 1 OF 1